PHILOSOPHICAL TRANSACTIONS OF THE ROYAL SOCIETY A MATHEMATICAL, PHYSICAL & ENGINEERING SCIENCES

Micromechanisms of Flow and Fracture, and their Relevance to the Rheology of the Upper Mantle [and Discussion]

M. F. Ashby, R. A. Verrall, H. H. Schloessin, E. H. Rutter, K. H. G. Ashbee, S. H. White, S. A. F. Murrell and A. Kelly

Phil. Trans. R. Soc. Lond. A 1978 **288**, 59-95
doi: 10.1098/rsta.1978.0006

Phil. Trans. R. Soc. Lond. A. **288**, 59–95 (1977) [59]
Printed in Great Britain

Micromechanisms of flow and fracture, and their relevance to the rheology of the upper mantle

By M. F. Ashby and R. A. Verrall
Cambridge University, Engineering Department, Trumpington Street, Cambridge CB2 1PZ

Crystalline solids respond to stress by deforming elastically and plastically, and by fracturing. The dominant response of a given material depends on the magnitude of the shear stress (σ_s), on the temperature (T) and on the time (t) of its application. This is because a number of alternative mechanisms exist which permit the solid to flow, and its fracture, too, occurs by one of a number of competing mechanisms. Their rates depend on σ_s, T and t: it is the fastest one which appears as dominant.

In geophysical problems, pressure appears as an additional variable. At pressures corresponding to depths of a few kilometres below the surface of the Earth, the mechanisms of fracture are the most affected; but at depths of a few hundred kilometres, plasticity, too, is influenced in important ways.

This paper outlines the mechanisms of flow and fracture which appear to be relevant in the deformation of materials of interest to the geophysicist, and the way pressure affects them. The results are illustrated and their shortcomings emphasized by using them to calculate the mechanisms of flow and fracture to be expected in the upper mantle of the Earth.

1. Introduction

1.1. *Micromechanisms of flow and fracture*

There exist a number of alternative mechanisms by which a crystalline solid may deform or fracture. At low temperatures, it may fracture by *cleavage* before it yields. It may yield or twin, exhibiting *low-temperature plasticity*, terminated by one of several sorts of *ductile fracture*. As the temperature is raised, the solid may start to flow by *power-law creep*, and even, at sufficiently high temperatures, by *diffusional flow*, until it fails by one of a number of *creep fracture* processes.

Although none of these is completely understood, the underlying physics is sufficiently clear that each can be modelled approximately. The models lead to *constitutive laws*: equations relating the strain increment (or strain-rate) to the stress and temperature applied to the solid, and to the time. These constitutive laws, when fitted to experimental data, give a useful description of the mechanisms of flow or fracture in a form which can be used for solving boundary-value problems.

In materials science and engineering, it is uncommon to regard the hydrostatic pressure as an independent variable: it is almost always determined by the shear strength of the material and seldom exceeds 1 % of its bulk modulus (K). Because of this, the effect of pressure on mechanical strength is less studied than the effect of, say, temperature. However, in many geophysical problems, pressure is as important a variable as temperature, and at great depths below the Earth's surface, the pressures are immense: at a depth of 400 km, for instance, the pressure is about $K/10$.

Even small pressures ($K/100$ or less) have a large effect on mechanisms of fracture. A superimposed pressure of the same magnitude as the yield strength, for example, suppresses most

modes of ductile fracture. Cleavage fracture is an exception: as described in § 3, even a large pressure does not suppress it entirely, though it may make it so difficult that some other mechanism of flow appears instead.

Plasticity and creep are much less affected by pressures. In engineering design, it is normal to assume that it is only the shearing, or *deviatoric*, part of the stress field which causes flow; pressure has no effect whatever. There is some justification for this: neither low-temperature plasticity nor creep are measurably affected by pressures less than $K/100$. But when the pressure exceeds this value, the rates of flow are slowed, and pressure must be regarded, with the temperature and shear stress, as an independent variable.

1.2. *Mechanisms important in geophysical modelling*

In understanding and modelling phenomena such as the flow of the Earth's mantle, or the creep of a large ice body, or formation of a salt dome, it is important to identify the dominant mechanism of deformation, since this determines how the strains (and thus, displacements) are related to the stress and temperature. We shall consider as an example the mechanisms involved in the first of these problems, but the same mechanisms and method could be applied equally well to the other two.

Geophysical and petrologic evidence suggest that the dominant phase in the upper mantle is olivine Fo_{85}–Fo_{95} (Fo_{85} is $(Mg_{0.85}Fe_{0.15})_2SiO_4$) (Birch 1969; Ringwood 1970), so that, as a first approximation, the upper mantle can be treated rheologically as pure olivine. (There are certain risks in this: in the low velocity zone, a shell of the upper mantle about 150 km below the surface, a basaltic phase in the mantle rock may melt, locally changing the mechanical behaviour. Flow in the presence of a fluid phase cannot yet be modelled adequately, but it is discussed in § 7.)

The mechanisms responsible for steady-state deformation in the upper mantle have been considered by several authors (Gordon 1965, 1967; McKenzie 1968; Weertman 1970; Raleigh & Kirby 1970; Carter & Ave' Lallemant 1970; Stocker & Ashby 1973). This paper extends the earlier work. In particular, it includes cataclastic flow as a mechanism; it incorporates recent developments in the understanding of plastic flow and creep and in the way in which pressure affects them; and it reviews and uses new data on the transport and mechanical properties of olivine.

The mechanisms which appear to be most important in such problems are:

(*a*) *Cataclastic flow* (§ 3): to a materials scientist, this is not flow, but fracture. It is modelled as repeated cleavage fracture together with the rolling of already fragmented particles over each other.

(*b*) *Low-temperature plasticity* (§ 4): plastic deformation involving the gliding motion of dislocations.

(*c*) *Diffusional flow* (§ 5): deformation by the diffusive motion of single ions, possible only at high temperatures, and leading to flow which is, at least approximately, Newtonian viscous.

(*d*) *Power-law creep* (§ 6): a non-linear flow involving both the climb and glide motion of dislocations.

There exist several other mechanisms – twinning, for instance – which we do not understand well enough to model in detail. Two of these are clearly of importance in the deformation of the Earth's crust and mantle, and are the major gaps in our present understanding. They are:

(*e*) *Fluid-phase transport* (§ 7): flow in the presence of an aqueous fluid phase or a partial melt.

(*f*) *Creep with dynamic recrystallization* (§ 7): creep accelerated, or made possible, by continuous recrystallization.

Throughout the paper we are concerned with steady-state flow. When strains are small ($< 10^{-2}$), as they are when the upper mantle deforms in response to surface loads, for instance, transient effects cannot be neglected (Goetze 1971). When the strains are large ($\geqslant 1$), as they are in mantle convection, the contribution of transients depends on how rapidly the stress and temperature change along a stream path; but for all but the most rapidly changing conditions, the assumption of steady-state flow is a good first approximation.

TABLE 1. MATERIAL PROPERTIES FOR OLIVINE

material property	symbol	value	units	remarks
molecular volume per oxygen ion at 1 atm.†	Ω^0	1.23×10^{-29}	m^3	This value used for diffusional flow, equation (5.1)
oxygen ion volume at 1 atm.	Ω_i^0	1.15×10^{-29}	m^3	This value used for activation volumes, equation (5.9).
Burgers vector at 1 atm.	$\boldsymbol{b}^0$	6.0×10^{-10}	m	An average of several values – § 4
melting point at 1 atm.	T_M	2140	K	
shear modulus at 300 K and 1 atm.	μ^0	8.13×10^{10}	Pa	See §§ 2.2 and 2.3 for references
T-dependence of shear modulus	$(T_M/\mu^0)(d\mu/dT)$	0.35	—	
P-dependence of shear modulus	$d\mu/dP$	1.8	—	
bulk modulus at 300 K and 1 atm.	K^0	1.27×10^{11}	Pa	See §§ 2.2 and 2.3 for references
T-dependence of bulk modulus	$(T_M/K^0)(dK/dT)$	0.26	—	
P-dependence of bulk modulus	dK/dP	5.1	—	
pre-exponential, lattice diffusion	D_{ov}	0.1	m^2/s	The data are discussed in § 5 and plotted in figure 9
activation energy, lattice diffusion	Q_v	522	kJ/mol	
activation volume/oxygen ion volume	V^*/Ω_i	0–1	—	
pre-exponential, boundary diffusion	δD_{OB}	1×10^{-10}	m^3/s	There are no data for olivine.
activation energy, boundary diffusion	Q_B	350	kJ/mol	These are obtained by scaling: $\delta D_{OB} = 10^{-9} D_{ov}$ and $Q_B = \frac{2}{3} Q_v$
activation volume/oxygen ion volume	V^*/Ω_i	0–1	—	
first creep exponent	n_1	3	—	See § 6.4 for the rate equation used for power-law creep. The values refer to creep in shear (equation (6.4))
second creep exponent	n_2	5	—	
first creep constant	A_1	0.45	—	
second creep constant	A_2	5.4×10^4	—	Q_{cr} and V^*_{cr} are the same as those for lattice diffusion
activation energy for creep	Q_{cr}	522	—	
activation volume/oxygen ion volume	V^*_{cr}/Ω^0	0–1		
flow stress at 0 K, (lattice resistance)/modulus	τ_p/μ	3.3×10^{-2}	—	This determines the flow stress at 0 K and throughout the plasticity field – see also § 4
pre-exponential for lattice resistance	$\dot{\gamma}_p$	10^{11}	s^{-1}	
activation energy for lattice resistance	$\Delta F_p/\mu b^3$	0.05	—	
flow stress at 0 K, (obstacle control)/modulus	$\hat{\tau}_0/\mu$	8×10^{-3}	—	This determines the plateau in the flow stress separating plasticity from power-law creep – see also § 4
pre-exponential, obstacle control	$\dot{\gamma}_0$	10^6	s^{-1}	
activation energy for obstacle control	$\Delta F_0/\mu b^3$	0.5	—	
cleavage stress in tension modulus	σ_t/μ	5×10^{-3}	—	See § 3 and table 4

† 1 atm $\approx 10^5$ Pa.

PHILOSOPHICAL TRANSACTIONS OF THE ROYAL SOCIETY A MATHEMATICAL, PHYSICAL & ENGINEERING SCIENCES

The following sections give, with explanation, a simple constitutive law for each mechanism of flow, including the effects of pressure. They have the form

$$\dot{\gamma} = f(\sigma_s, p, T, M_1, M_2, \ldots), \tag{1.1}$$

where $\dot{\gamma}$ is the shear strain-rate, σ_s the shear stress, p the hydrostatic pressure, T the absolute temperature, and M_1, M_2, etc., are material properties. Each section contains a discussion of the material properties for olivine; they are summarized in table 1, which also serves to define the symbols. In a later section (§ 8) the equations and data are used to construct deformation-mechanism maps for olivine, both under laboratory conditions (constant pressure) and under the conditions presumed to obtain in the upper mantle.

It is worth pointing out that, for all the mechanisms except cataclastic flow, pressure enters the laws only through the influence on the material properties (M_1, M_2, etc.). For these mechanisms one may write

$$\dot{\gamma} = f(\sigma_s, T, M_1(p), M_2(p) \ldots).$$

Because pressure enters in this way, the Prandtl–Reuss generalization still applies, and the equation can be written in a form suitable for numerical computation:

$$\mathrm{d}\varepsilon_{ij}/\mathrm{d}t = f(\bar{\sigma}_s, T, M_1(p), M_2(p) \ldots)\, S_{ij}/2\bar{\sigma}_s, \tag{1.2}$$

where the function f is the same as before. Here $\mathrm{d}\varepsilon_{ij}$ are the components of the strain increment, $\mathrm{d}t$ is the increment of time, and $\bar{\sigma}_s$ is an equivalent shear stress:

$$\bar{\sigma}_s^2 = \tfrac{1}{6}[(\sigma_1-\sigma_2)^2+(\sigma_2-\sigma_3)^2+(\sigma_3-\sigma_1)^2] = \tfrac{1}{2}S_{ij}S_{ij}; \tag{1.3}$$

p is the hydrostatic pressure:

$$p = -\tfrac{1}{3}(\sigma_1+\sigma_2+\sigma_3) = -\tfrac{1}{3}\sigma_{kk}; \tag{1.4}$$

and S_{ij} is the deviatoric part of the stress tensor:

$$S_{ij} = (\sigma_{ij} - \tfrac{1}{3}\delta_{ij}\sigma_{kk}). \tag{1.5}$$

The quantities σ_1, σ_2 and σ_3 are the principal stresses, and σ_{ij} is the stress tensor.

It is not permissible to generalize equations for fracture in this way because pressure enters the equations directly, not merely through its influence on a material property.

For later use, it is convenient to define an equivalent shear strain-rate:

$$\bar{\dot{\gamma}}^2 = \tfrac{2}{3}[(\dot{\epsilon}_1-\dot{\epsilon}_2)^2+(\dot{\epsilon}_2-\dot{\epsilon}_3)^2+(\dot{\epsilon}_3-\dot{\epsilon}_1)^2] = 2\dot{\epsilon}_{ij}\dot{\epsilon}_{ij}, \tag{1.6}$$

where $\dot{\epsilon}_1$, $\dot{\epsilon}_2$, and $\dot{\epsilon}_3$ are the principal strain-rates, and $\dot{\epsilon}_{ij}$ is the strain-rate tensor.

2. Effect of pressure and temperature on ionic volumes and moduli

2.1. *Effect of pressure on the ionic volume and Burgers vector*

In a linear-elastic solid of bulk modulus K^0, the atomic or ionic volume varies with pressure as

$$\Omega = \Omega^0 \exp\{-(p-p^0)/K^0\}, \tag{2.1}$$

and the lattice parameter a (and the Burgers vector $\boldsymbol{b}$) as

$$a = a^0 \exp\{-(p-p^0)/3K^0\}, \tag{2.2}$$

where Ω^0 and a^0 (or b^0) are the values at atmospheric pressure (p^0). Their change with temperature is sufficiently small that we can safely neglect it. Data for Ω^0, b^0 and K^0 for olivine are given in table 1.

2.2 *Effect of temperature and pressure on the moduli*

To first-order, the moduli increase linearly with pressure and decrease linearly with temperature. We write this in the form

$$\mu = \mu^0\left\{1-\left[\frac{T_M}{\mu^0}\frac{d\mu}{dT}\right]\frac{(T-300)}{T_M}\right\}+\left[\frac{d\mu}{dp}\right](p-p^0); \tag{2.3}$$

$$K = K^0\left\{1-\left[\frac{T_M}{K^0}\frac{dK}{dT}\right]\frac{(T-300)}{T_M}\right\}+\left[\frac{dK}{dp}\right](p-p^0), \tag{2.4}$$

where p^0 is atmospheric pressure, which, for almost all practical purposes, we can ignore.

The coefficients in the square brackets are dimensionless. Table 2 lists means and standard deviations of the temperature coefficients for a number of cubic elements and compounds. Most are metals, though data for some alkali halides and oxides are included; data for olivine are listed separately. The dimensionless coefficients are roughly constant. When no data are available these mean values can be used.

TABLE 2. TEMPERATURE COEFFICIENTS OF THE MODULI

coefficient	number of materials	mean and s.d.	source of data	value for olivine	reference
$\left[\frac{T_M}{\mu^0}\frac{d\mu}{dT}\right]$ $(\mu=\{\frac{1}{2}C_{44}(C_{11}-C_{12})\}^{\frac{1}{2}})$	11	0.52 ± 0.1	Frost & Ashby (1973)	0.35	Kamazama & Anderson (1969)
$\left[\frac{T_M}{K^0}\frac{dK}{dT}\right]$ $(K=\frac{1}{3}(C_{11}+2C_{12}))$	9	0.36 ± 0.2	Huntington (1958)	0.26	Huntington (1958)

TABLE 3. PRESSURE COEFFICIENTS OF THE MODULI

material	$10^{-10}\mu^0$/Pa	$10^{-10}K^0$/Pa	$\left[\frac{d\mu}{dp}\right]$	$\left[\frac{dK}{dp}\right]$	$\frac{K^0}{\mu^0}$	$\left[\frac{K^0}{\mu^0}\frac{d\mu}{dp}\right]$	reference
Al	2.54	7.3	2.2	3.9	2.87	6.3	Huntington (1958), Birch (1966)
Ag	2.64	10	2.3†	6.2‡	3.79	8.8	
Au	—	17.3	1.8†	6.4‡	—	—	
Cu	4.21	13.8	1.4	4.9	3.28	4.6	
Ni	7.89	18.3	1.5	—	2.37	3.6	
Na	0.23	0.83	1.6†	3.6‡	3.61	5.9	
Li	0.35	1.3	1.0†	—	3.71	—	
αFe	6.4	16.8	1.9	4.0	2.63	5.0	
Ge	5.2	7.73	1.3†	4.7‡	1.49	2.0	
Si	6.37	9.88	0.8†	4.2‡	1.55	1.2	
NaCl	1.51	2.35	2.7†	6.0‡	1.56	4.2	
LiF	4.58	7.0	1.4	—	1.53	2.2	
MgO	—	16.7	2.6	3.9	—	—	
SiO_2	—	3.7	2.9†	—	—	—	
Mg_2SiO_4	8.13	12.7	1.8	5.1	1.56	2.8	Graham & Barsch (1969), Kamazama & Anderson (1969)
mean and s.d.			1.8 ± 0.7	4.8 ± 1	2.5 ± 1	4.3 ± 2	

† This is dC_{44}/dp. ‡ This is $d(\frac{1}{3}(C_{11}+2C_{12}))/dp$.

Table 3 lists the moduli and their pressure-dependence for a number of materials, including olivine. Again, the dimensionless coefficients are roughly constant; for materials for which no data are available, it is reasonable to use the mean values indicated at the foot of the table.

3. Cataclastic flow by cleavage and by rolling-plus-sliding

Almost all crystalline solids are capable of fracture by cleavage if the temperature is sufficiently low; the f.c.c. metals and their alloys appear to be the only exceptions. A confining pressure makes cleavage more difficult but does not necessarily prevent it. It is therefore possible to develop large shearing displacements in a brittle solid, constrained by a pressure, by a process of repeated fracturing, or *cataclasis*.

Once fracturing has started, so that the material has become fragmented, continued shearing may simply break the fragments into ever smaller pieces. But there is an alternative: shearing can continue if the fragments slide and roll over each other.

Simple, and approximate, models for these two alternative processes are considered in this section. From them we learn that rolling is more pressure-sensitive than repeated fracturing, which always becomes the dominant of the two processes when the confining pressure is large.

3.1. *Cleavage fracture*

The tensile stress which will overcome the interatomic forces in a perfect crystal, causing it to separate on a plane normal to the stress axis, defines an upper limiting strength for a crystalline solid. The many calculations of it are in general agreement (Kelly 1966; Macmillan 1972): at an adequate level of accuracy

$$\sigma_{\text{ideal}} = (2E\Gamma_s/\pi b)^{\frac{1}{2}} \approx 0.1\,E, \tag{3.1}$$

where Γ_s is the surface free energy, E is the Young modulus and b is the atomic size. Fracture occurs when the tensile stress exceeds σ_{ideal}.

The ideal strength is rarely realized. Almost always, small cracks pre-exist in brittle and semi-brittle solids, or are created in them by slip as soon as yielding occurs. Such a crack concentrates stress, so that the ideal strength is exceeded at its tip when the applied stress is still much less than σ_{ideal}.

The stress at the tip of an atomically sharp crack of length $2C_0$ in an elastic medium can be calculated: it is $(C_0/b)^{\frac{1}{2}}$ times larger than the applied stress. If the crack propagates when the ideal strength is exceeded at its tip, the fracture stress in simple tension obviously becomes

$$\sigma_f = (2E\Gamma/\pi C_0)^{\frac{1}{2}}, \tag{3.2}$$

a result first developed by Griffith (1924) using an energy argument, and later by Orowan (1934, 1949) using an argument based on stresses (as here). In this equation, 2Γ is the energy absorbed per unit area of crack advance; its minimum value is $2\Gamma_s$. One could, then, describe the cleavage-fracture strength of a material by citing the values of C_0 and Γ which characterize it. But for brittle minerals and rocks this is impractical; it is much easier to treat σ_f, the stress at which cleavage fracture occurs in simple tension, as the material property, and use it to calculate the conditions for fracture under pressure.

3.2. *Effects of pressure*

Griffith (1924) himself extended the fracture criterion to include the effect of biaxial stress states. A material can fracture by cleavage, even when the stress state is a compressive one, because cracks orientated at an angle to the compression axis are loaded in shear, and therefore have regions of tension and compression at their tips, as illustrated in figure 1. Suppose cracks of equal size, in a biaxial stress field, are assumed to have their planes parallel to the unstressed direction, but are otherwise orientated at random. A tensile component in the applied stress will tend to open some of the cracks; but even if the stress field is compressive, any deviatoric component in it will tend to make some cracks slide.

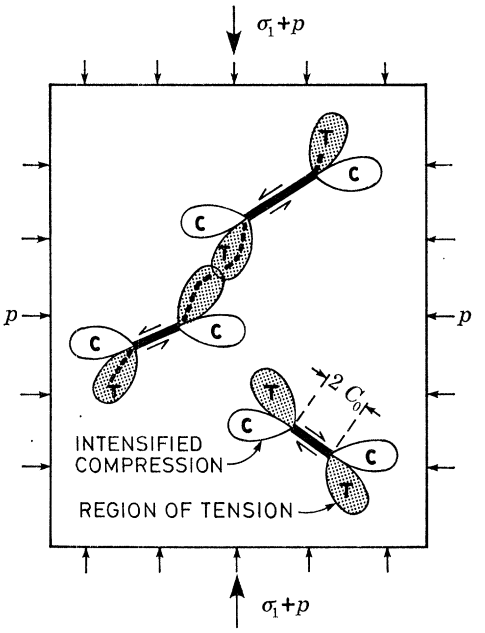

FIGURE 1. Cataclastic flow by cleavage. A deviatoric stress causes shearing displacements across the crack faces, generating tensile stresses in the regions marked *T*. If these reach a critical level, the cracks extend (broken lines) and ultimately link, even when the stress field is a compressive one.

In either case, a tensile stress appears at the crack tip. Its magnitude can be calculated as a function of the angle of orientation of the crack, assuming the crack faces to be frictionless. If fracture occurs when the maximum value of this stress exceeds σ_{ideal}, then the Griffith fracture criterion becomes (after McClintock & Argon 1966)

$$\left.\begin{aligned} \sigma_1 &= \sigma_f \quad \text{if} \quad -3\sigma_f \leqslant \sigma_3 \leqslant \sigma_1; \\ (\sigma_1-\sigma_3)^2+8\sigma_f(\sigma_1+\sigma_3) &= 0 \quad \text{if} \quad \sigma_3 < -3\sigma_f, \end{aligned}\right\} \tag{3.3}$$

where σ_1 is the largest (most tensile) and σ_3 the smallest principal stress.

McClintock & Argon (1966) argue that, in a triaxial field ($\sigma_1 > \sigma_2 > \sigma_3$) the intermediate principal stress σ_2 does not change the criterion. Cracks with normals in the $\sigma_1-\sigma_3$ plane are exposed both to the largest tensile and largest shear stress; and (in an elastic solid) a normal stress σ_2 in the crack plane is not concentrated by the crack. The criterion above is then unaltered.

The model predicts that the fracture strength in compression should be 8 times larger than that in tension. Tests on rocks and minerals show it to be between 8 and 15 times larger (Jaeger & Cook 1969), so while it is a useful approximation the model is incomplete. There are two deficiencies. First, crack-plane friction is ignored. It can be included (McClintock & Walsh 1962) but the coefficient of friction required to fit experiment is unexpectedly large, perhaps because the crack faces are serrated, and key together when under compression. More important, the crack, when it extends under compression, deviates from the plane originally containing it. Equation (3.3) is an initiation condition, not a criterion for propagation. Final fracture in compression requires an understanding of the interaction between cracks that we do not yet possess. It seems likely that the propagation conditions will depend on pressure in the same way as the initiation condition does, and (as figure 1 suggests) that the two conditions merge when the initial density of cracks is high; but there is no proof of this, and we must treat it as a postulate.

Assuming this to be true, the fracture criterion for shear with a superimposed hydrostatic pressure becomes, when expressed in terms of the shear stress σ_s and the hydrostatic pressure p:

$$\left.\begin{aligned} \sigma_s &\geqslant \sigma_f + p \quad \text{if} \quad p < \sigma_f; \\ \sigma_s &\geqslant 2(\sigma_f p)^{\frac{1}{2}} \quad \text{if} \quad p \geqslant \sigma_f, \end{aligned}\right\} \tag{3.4}$$

where $\sigma_s = \frac{1}{2}(\sigma_1 - \sigma_2)$, $p = -\frac{1}{3}(\sigma_1 + \sigma_2 + \sigma_2)$, and the principal stresses are $p + \sigma_s$, p, and $p - \sigma_s$. Equations (3.4) are plotted in figure 2, which shows how the deviatoric stress required to cause cleavage rises as the pressure increases. Note that cleavage is possible when the confining pressure is large, provided that the shear stress, too, is large.

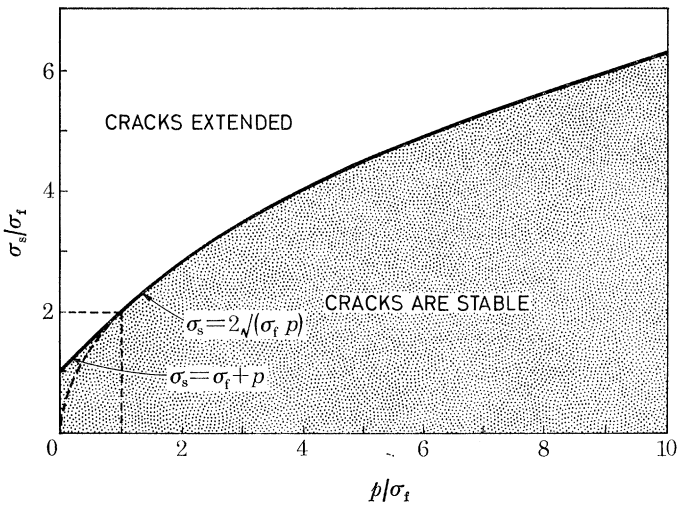

FIGURE 2. Griffith criterion, no friction. A plot of equations (3.4), showing how the deviatoric stress required to cause cleavage (or cataclasis) increases with pressure; σ_f is the fracture strength in tension.

3.3. *Fracture data for olivine*

The material property which appears in equations (3.4) is the fracture strength in tension, σ_f. Values for olivine-containing rocks can be deduced from two sources: the tests of Griggs, Turner & Heard (1960) on dunite, and those of Handin (1966) on peridotite. Both were compressive tests, with a confining pressure. We have used equation (3.3) to calculate the material

property, σ_f from their data. The results are tabulated in table 4. In the later calculations of this paper, we have used the value of $\sigma_f = 5 \times 10^{-3}\,\mu$ (table 1).

3.4. *Rate law for cataclastic flow*

We have modelled cataclastic flow as the result of two independent mechanisms. First we assumed extensive flow is possible by fracturing if equation (3.4) is satisfied; in fracturing, the rock becomes increasingly granulated. Secondly, we assumed that extensive flow is also possible by the rolling and sliding (without further fracture) of the granulated rock. The model for this second process is of the simplest and most approximate kind, and is illustrated by figure 3.

TABLE 4. LOW-TEMPERATURE FRACTURE OF DUNITE AND PERIDOTITE

T/°C	T/T_M	σ_1/MPa	σ_3/MPa	σ_f/MPa	$10^3\sigma_f/\mu$	reference
25	0.14	500	2300	650	8.1	Griggs *et al.* (1960)
25	0.14	500	2000	500	6.2	
150	0.2	100	510	400	5.0	Handin (1966)
150	0.2	100	450	350	4.5	

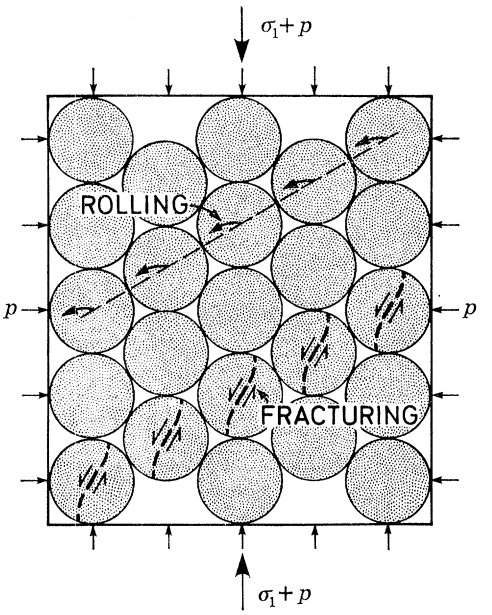

FIGURE 3. Granular or previously fractured materials can deform by the rolling and sliding of the granules or fragments over each other. Such flow is associated with a volume expansion, and because of this, it is more strongly influenced by pressure than is cleavage.

Consider the granules to be cylinders which roll and slide at their points of contact. When the array is sheared, it expands, doing work against the confining pressure and dissipating energy in overcoming friction at points of contact, some of which must slide. This work must be supplied by the applied shear stress. If the cylinders form a close-packed array, the largest stress is that needed to start them shearing; thereafter they will continue to shear. It is easy to show that this requires

$$\sigma_s \geqslant p\,(\tfrac{1}{\sqrt{3}} + \sqrt{3}\,\mu_f), \tag{3.5}$$

where the first term in the parentheses derives from the work done in dilating the material against the confining pressure p, and the second is the work done against friction (coefficient of friction μ_f). The term in parentheses is of order 1, and remains so when the model is broadened to describe the rolling of spheres instead of cylinders. Because of its more rapid dependence on p, rolling is suppressed by even modest pressures, and is replaced by the fracturing mode of flow.

Cataclastic flow is incorporated into the calculations of Section 8 by assuming that:

$$\left.\begin{aligned}\dot{\gamma} &= \infty \text{ if either the rolling or fracturing criteria (equations (3.4) or (3.5)) is satisfied,}\\ \dot{\gamma} &= 0 \text{ if neither is satisfied.}\end{aligned}\right\} \quad (3.6)$$

4. Low-temperature plasticity

At low temperatures, or high rates of strain, plastic flow in crystalline solids is by slip. Dislocations – the 'carriers' of deformation – glide on slip planes; the combination of a plane and a Burgers vector defining a slip system. If a polycrystal is to deform homogeneously without fracturing, five independent slip systems must be available; but if non-homogeneous deformation is allowed, so that although grains deform compatibly, they do not deform uniformly, then four systems may be sufficient (Hutchinson 1976, private communication). This mechanism, which we shall call low-temperature plasticity, is illustrated by figure 4.

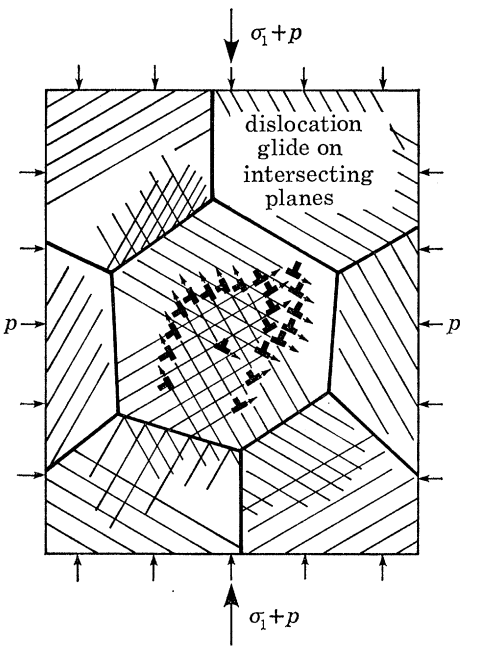

Figure 4. Low-temperature plasticity. The gliding motion of several sets of dislocations permits compatible deformation of the grains of a polycrystalline solid.

4.1. *Lattice-resistance and obstacle-controlled plasticity*

Dislocations glide in many pure metals with great ease, and for that reason they are often very soft. But in rocks and minerals this is not so. Many, like the silicates, are covalently bonded, and the covalent bond is hard to break. The result is that the energy of the crystal fluctuates when the dislocation moves (figure 5, top), and a force which is proportional to the slope of the energy–distance curve is required to make it do so.

Obstacles – impurities, precipitates, other dislocations, and so forth – obstruct glide also; but their effect is observable only if the energy hill they place in the path of the moving dislocation is steeper than that due to bond breaking (figure 5, bottom). Sometimes this is so, and the flow strength of the crystal (which reflects an average of the behaviour of dislocations on four or five slip systems) is said to be obstacle controlled. When it is not, the flow stress is lattice-resistance controlled.

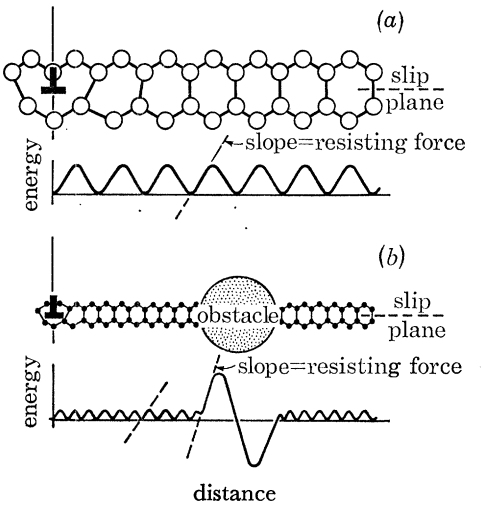

FIGURE 5. The yield strength reflects the force required to move a dislocation. In silicates such as olivine, the structure itself resists the motion, and the strength is said to be 'lattice resistance controlled' (*a*). Strong discrete obstacles – such as other dislocations – can sometimes determine the yield strength, which is then said to be 'obstacle-controlled' (*b*).

Above 0 K, thermal energy is available. It is then possible, by a straightforward application of kinetic theory, to calculate the average drift velocity of dislocations through the crystal, and hence the strain rate. The details of the calculation and of the result depend on the shape of the energy hills of figure 5 (see, for example, Kocks, Argon & Ashby 1976). That which best fits the available experimental data for lattice-resistance controlled glide leads to the rate equation

$$\dot{\gamma} = \dot{\gamma}_{\mathrm{p}} \left(\frac{\sigma_{\mathrm{s}}}{\mu}\right)^2 \exp\left\{-\frac{\Delta F_{\mathrm{p}}}{kT}\left(1-\left(\frac{\sigma_{\mathrm{s}}}{\hat{\tau}_{\mathrm{p}}}\right)^{\frac{3}{4}}\right)^{\frac{4}{3}}\right\}, \tag{4.1}$$

where $\dot{\gamma}_{\mathrm{p}}$ is a pre-exponential rate-constant, ΔF_{p} is the activation energy for lattice-resistance controlled glide, and $\hat{\tau}_{\mathrm{p}}$ represents the flow stresses at 0 K.

Because of the small activation energy (ΔF_{p}) the strengthening caused by the lattice resistance drops as the temperature is raised, until its contribution becomes less than that of discrete obstacles (figure 5, lower drawing). When they control the flow stress, flow is better described by the simpler equation

$$\dot{\gamma} = \dot{\gamma}_0 \exp\{(-\Delta F_0/kT)\,(1-\sigma_{\mathrm{s}}/\hat{\tau}_0)\}, \tag{4.2}$$

where $\dot{\gamma}_0$ is the pre-exponential rate-constant, ΔF_0 the activation energy for cutting or passing the obstacle, and $\hat{\tau}_0$ is the flow stress at 0 K if the obstacles acted alone. In later calculations, we select the slower of these two strain-rates: both lattice resistance and obstacle must be overcome, and it is the more difficult of the two which determines the strength.

Dislocation glide is characterized by a long transient (work hardening), which continues until a saturation flow stress is reached. In tensile tests, fracture occurs before saturation, and,

because of this, dislocation glide is not usually thought of as a steady-state mechanism of flow. But experiments in torsion or compression suggest that a saturation flow stress is ultimately reached, though the strains involved are large (> 1).

4.2. *Effect of pressure on low-temperature plasticity*

High strength materials have a yield strength in tension which is lower than that in compression – a phenomenon known as the 'strength differential' (s-d) effect. Recent experimental studies of high strength steels (Spitzig, Sober & Richmond 1975, 1976) have shown that this is simply the effect of pressure on the flow stress. Some of their data are replotted in figure 6, which shows how the shear strength σ_s of a steel at room temperature increases linearly with pressure. The axes of this figure have been normalized: the ordinate by dividing σ_s by σ_s^0 (the value at $p = 0$) and abscissa by dividing p by the bulk modulus, K^0. The slope is a useful dimensionless measure of the pressure-dependence of the yield strength. For this steel, and for two others studied by Spitzig *et al.*, the slope was

$$\mathrm{d}(\sigma_s/\sigma_s^0)/\mathrm{d}(p/K^0) = 6\text{–}10. \tag{4.3}$$

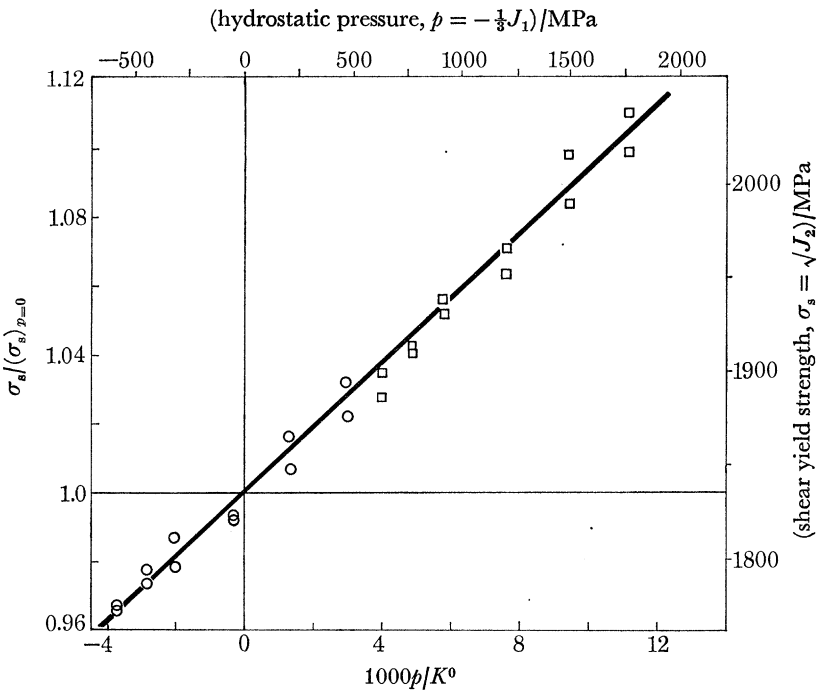

FIGURE 6. The pressure-dependence of the yield strength of a maraging steel. The yield strength increases linearly with pressure. The data are replotted from Spitzig, Sober & Richmond (1976): ○, tension; □, compression; slope = 9.3.

The effect is far too large to be accounted for by the permanent volume expansion associated with plastic flow and must be associated instead with a direct effect of pressure on the motion of dislocations.

This pressure-dependence can be accounted for almost entirely by considering the effect of pressure on the activation energies ΔF_p and ΔF_0 and the strengths $\hat{\tau}_p$ and $\hat{\tau}_0$. It is commonly found (see Kocks *et al.* (1976) for a review) that the activation energy for both obstacle and lattice-resistance controlled glide scales as μb^3 and that the strengths $\hat{\tau}$ scale as μ. For most b.c.c. metals,

for example, the activation energy is close to $0.07\,\mu b^3$ and the flow stress at absolute zero is close to 0.01μ (Frost & Ashby 1973). As already described, both μ and b depend on pressure, μ increasing more rapidly than b^3 decreases. Pressure, then, has the effect of raising both the activation energy and the strengths, $\hat{\tau}$.

At absolute zero, the shear stress required to cause flow is simply $\hat{\tau}$. Using equation (2.3) for the modulus, and neglecting the pressure p^0, we find by inserting the above proportionalities into equation (4.2),

$$\sigma_s = \hat{\tau}_0(p) = \sigma_s^0\left(1 + \left[\frac{K^0}{\mu^0}\frac{\mathrm{d}\mu}{\mathrm{d}p}\right]\frac{p}{K^0}\right), \tag{4.4}$$

from which

$$\mathrm{d}\left(\frac{\sigma_s}{\mu^0}\right)\Big/\mathrm{d}\left(\frac{p}{K^0}\right) = \left[\frac{K^0}{\mu^0}\frac{\mathrm{d}\mu}{\mathrm{d}p}\right]. \tag{4.5}$$

Values of this dimensionless quantity are listed in table 3 for a variety of materials. The values range from 2 to 9 compared with the measured coefficient of 6 to 10, but the measurements, of course, were made at room temperature – about $0.2\,T_M$ for many of the listed materials.

As the temperature is raised the picture becomes more complicated. The flow stress becomes, on inverting equation (4.2),

$$\sigma_s = \hat{\tau}_0(p)\,\{1 - [kT/\Delta F_0(p)]\ln(\dot{\gamma}_0/\dot{\gamma})\}, \tag{4.6}$$

in which both $\hat{\tau}_0$ and ΔF_0 increase with pressure, so that at fixed T and $\dot{\gamma}$, the predicted pressure dependence of σ_s *increases* with increasing temperature, and adequately accounts for the observed effects.

There are other contributions to the pressure-dependence of low-temperature plasticity, but they appear to be small. The presence of a dislocation expands a crystal lattice, partly because the core has a small expansion associated with it (about $0.5\,\Omega$ per atom length) and partly because the non-linearity of the moduli cause any elastic strain-field to produce an expansion (Seeger 1955; Lomer 1957; Friedel 1964). It is this second effect which is, in general, the more important. The volume expansion is roughly

$$V^* = \tfrac{3}{2}\Delta E^{\mathrm{el}}/\mu \quad \text{per unit volume,} \tag{4.7}$$

where ΔE^{el} is the elastic energy associated with the strain-field. If the activation energy which enters the rate equations is largely elastic in origin, (as it appears to be) then during activation, there is a small temporary increase in volume, V^*. A pressure further increases ΔF by the amount pV^*. Because they are small, these contributions are neglected in the present treatment.

4.3. *Low-temperature plasticity of olivine*

The slip systems in olivine deformed at temperatures up to 1250 °C have been determined by electron microscopy (Phakey, Dollinger & Christie 1972) and optical examination (Raleigh 1968; Carter & Ave' Lallemant 1970; Young 1969; Raleigh & Kirby 1970). The review by Paterson (1974) gives details of the primary and secondary slip systems, and of how temperature affects their ease of operation and influences the resulting dislocation arrays. At 1000 °C and below, Phakey *et al.* (1972) observed straight dislocations, suggesting a large lattice resistance; but above 1250 °C, they saw subgrains of the kind associated with power-law creep.

The slip system which operates easily at low temperatures is that involving dislocations with $b = 5.98\,[001]$ Å gliding on (100) planes. If this slip system is suppressed by proper orientation of the crystal, then dislocations with Burgers vector $b = 4.76\,[100]$ Å gliding on (010) planes

appear. At 1000 °C these two systems operate with equal ease. Dislocations with a large Burgers vector ($\boldsymbol{b} = 10.21$ [010] Å on (100)) appear above 800 °C, particularly in crystals orientated so that the easy slip system is unstressed.

The calculations of § 8 require a value for the Burgers vector, though its value is not critical: it is used largely as a scaling parameter. We have used $\boldsymbol{b} = 6 \times 10^{-10}$ m (table 1) since this is broadly typical of the observations. Much more important are numerical values for the low temperature strength, since these are used to set the values of $\hat{\tau}$ and ΔF in equations (4.1) and (4.2). There are three sets of useful observations.

First, the yield stress for a peridotite (60–70 % olivine and 20–30 % enstatite) of grain size 0.5 mm, was measured by Carter & Ave' Lallemant (1970) between 325 and 740 °C. Secondly, Phakey *et al.* (1972) obtained stress–strain curves at 600 and 800 °C for single crystal forsterite. Four compression tests at 800 °C with different orientations of the single crystals produced yield stresses ranging from 570 to 1300 MN/m² (5.7–13 kbar). The highest value was obtained on the specimen orientated to produce no stress on the easy slip system; we have used this because it is the most representative of a polycrystalline material. Finally, some hardness data for olivine exists (Evans, cited by Durham & Goetze 1976), and it is this which gives the most complete picture of the low-temperature strength. It and the yield strengths are plotted on one of the deformation maps of § 8.

The quantities ΔF_p, $\hat{\tau}_p$ and $\hat{\tau}_0$ were obtained by fitting equations (4.1) and (4.2) to these data. We have assumed the frequency factor $\dot{\gamma}_0$ for olivine to be comparable with that for other materials with a large lattice resistance. The frequency factor $\dot{\gamma}_0$ and the activation energy ΔF_0 were also set by analogy with metals, but neither are important. The values used in later calculations are listed in table 1.

4.4. *Rate equations for low-temperature plasticity*

The later calculations of § 8 use the equations for lattice-resistance and obstacle-controlled glide as given in equations (4.1) and (4.2). The effects of pressure are included in exactly the way described above, by making ΔF scale as μb^3 and $\hat{\tau}$ as μ, and allowing μ and $\boldsymbol{b}$ to depend on both pressure and temperature as described in § 2. The consequences of doing so appear in the diagrams of § 8 and will be discussed there.

5. Diffusional flow

The plasticity described in the last section is observed at low temperatures and high stresses. Consider now the opposite extreme: flow at high temperatures and low stresses. Under these conditions metals and ceramics can deform by diffusion alone. Any deviatoric stress applied to them causes ions to flow by lattice diffusion or diffusion in the grain boundaries in such a way that the grains change their shape, permitting the stress to do work: it is this work that drives the diffusive flux. The resulting deformation is called diffusional flow, and is illustrated by figure 7.

5.1. *Diffusional flow*

Creep by diffusion alone can be modelled in detail. A compressive stress raises the chemical potential of ions on the boundaries of the grains. Provided that there is a difference in stress on these boundaries, and that atoms can be detached from them and reattached to them freely, matter will flow through or round the grains at a rate determined by diffusion.

Those who have calculated this rate (Nabarro 1948; Herring 1950; Lifshitz 1963; Raj &

Ashby 1971) are in general agreement: when both lattice diffusion and grain-boundary diffusion are permitted, the shear creep rate is

$$\dot{\gamma} = 42 D_{\text{eff}} \sigma_s \Omega / kTd^2, \tag{5.1}$$

where d is the grain diameter and Ω the atomic volume. D_{eff} is an effective diffusion coefficient, which, for a one-component system, is given by (see Raj & Ashby 1971):

$$D_{\text{eff}} = D_v[1 + (\pi\delta/d)\,(D_B/D_v)], \tag{5.2}$$

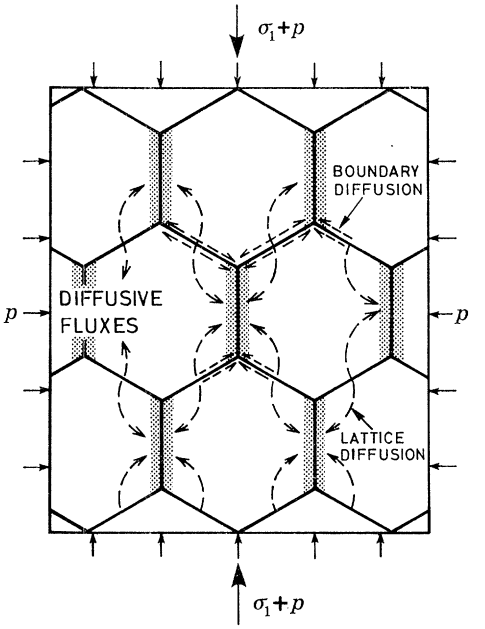

FIGURE 7. Diffusional flow. A deviatoric stress sets up differences in the chemical potential of ions at grain boundaries which then diffuse as shown by the broken lines, depositing in the shaded bands.

where D_v is the lattice self diffusivity, and δD_B that for boundary diffusion, multiplied by the thickness of the boundary diffusion path, δ. The equation describes a proper superposition of two submechanisms which are sometimes distinguished: when lattice diffusion dominates, it is called Nabarro–Herring creep; when, instead, boundary diffusion dominates, it is termed Coble creep. (The two sub-régimes are separated in the diagrams of § 8 by a vertical broken line.)

The quantities D_v, D_B and Ω are well defined in one-component solids. In pure copper, for instance, D_v is the lattice self-diffusion coefficient, D_B is the boundary self-diffusion coefficient, and Ω is the atomic volume. In a two-component system, their definition is more complicated. In ionic solids in which the diffusing species carry a charge, the appropriate diffusion coefficient for transport through the grain is (Lazarus 1971; Ruoff 1965):

$$D_v = \frac{D_v^A D_v^B}{(1-\chi_A) D_v^A + \chi_A D_v^B}, \tag{5.3}$$

where χ_A is the atom-fraction of A in the compound. The important point made by the equation is that it is the slower-moving component which determines the diffusion coefficient, and so limits the creep rate; a similar conclusion holds for systems with more than two components. In most oxides (including olivine) oxygen is the largest ion and the one which diffuses most slowly;

it is oxygen diffusion which will usually control the creep rate. (The silicon–oxygen bond in silicates may present special problems: it is so strong that oxygen might diffuse as an SiO_4^{4-} group, but measurements of creep and diffusion in olivine, reviewed below, do not support this view.)

The value of Ω, too, depends on the nature of the diffusing species. We shall assume that the diffusion of O^{2-} limits the rate of mass transport in olivine. Then, on average, the arrival of one oxygen ion at a grain boundary must be accompanied by $\frac{1}{4}$ of a silicon and $\frac{1}{2}$ of a magnesium or iron ion. Their total volume is $\frac{1}{4}$ of the molecular volume of $(Mg, Fe)_2SiO_4$ ($1.23 \times 10^{-29}\,m^3$); this is the quantity listed as Ω^0 in table 1, and used in equation (5.1). But if (although this seems very unlikely) diffusion involved the motion of SiO_4^{4-} units, then Ω^0 would become the entire molecular volume of $(Mg, Fe)_2SiO_4$.

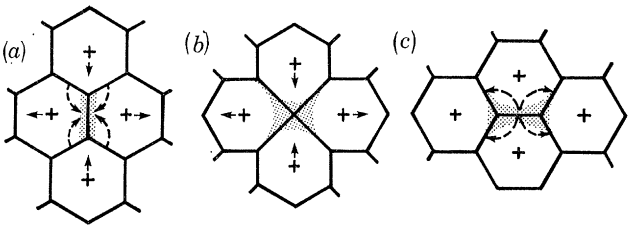

FIGURE 8. Diffusional flow when strains are large. If grains change their neighbours, the sample can undergo a large deformation while the grains alter their shape only slightly. At small strains (*a*) the diffusive paths, and the creep rate, are identical with those of figure 7, but at large strains ((*b*) and (*c*)) the paths differ and the rate is higher. Superplasticity in metals can be explained in this way.

Continuity of material during diffusional flow is maintained only if sliding displacements occur in the plane of the boundary; indeed, the mechanism can be regarded as diffusion-accommodated grain-boundary sliding (Raj & Ashby 1971), but it is a rather special form of this combined mechanism. It is implicit in the derivation of equation (5.1) that grains must suffer the same shape change as the specimen itself, and that they may not change their neighbours. When this constraint is relaxed (Ashby & Verrall 1972), a modified form of diffusional flow becomes possible: the grains slide past each other in the way illustrated by figure 8, changing neighbours and altering their shape (by diffusion) only where it is necessary for continuity to be maintained. This modified mechanism, which appears to be that underlying superplasticity in metals and ceramics, is simply a large-strain adaptation of the more familiar Nabarro–Herring and Coble creep. The rate equation describing it (see Ashby & Verrall 1973) closely resembles that given above. At a satisfactory level of approximation, it has the same form as equation (5.1), but is faster by a constant factor of about 5.

Diffusional flow, then, whether of the small-strain or the large-strain type, is controlled by the rate of diffusion of the slowest-moving species in the crystal. Pressure affects diffusional flow mainly because it slows the rate of diffusion.

5.2. *Effect of pressure on diffusional flow*

Pressure slows diffusion because it increases the energy required for an atom to jump from one site to another, and because it may cause the vacancy concentration in the solid to decrease. The subject has been extensively reviewed by Lazarus & Nachtrieb (1963), Girifalco (1964) and Peterson (1968); detailed calculations are given by Keyes (1963).

Steady-state diffusional flow requires that all atomic species in the material must move. This appears possible only by a vacancy mechanism, so we shall concentrate on this, and we shall further limit ourselves to pressures of less than $K/10$ – roughly the pressure at the base of the upper mantle.

The application of kinetic theory to self-diffusion by a vacancy mechanism (see, for example, Shewmon 1963) gives, for the diffusion coefficient

$$D = \alpha a^2 n_v \Gamma, \tag{5.4}$$

where α is a geometric constant of the crystal structure (independent of pressure) and a is the lattice parameter (weakly dependent on pressure in the way described by equation (2.2)). The important pressure-dependencies are those of the atom fraction of vacancies, n_v, and the frequency factor, Γ, which we discuss in order.

In a pure, one-component system, a certain atom fraction of vacancies is present in thermal equilibrium because the energy (ΔG_f per vacancy) associated with them is more than offset by the configurational entropy gained by dispersing them in the crystal. But in introducing a vacancy, the volume of the solid increases by V_f, and work pV_f is done against any external pressure, p. A pressure thus increases the energy of forming a vacancy without changing the configurational entropy, and because of this the vacancy concentration in thermal equilibrium decreases. If we take

$$\Delta G_f = \Delta G_f^0 + pV_f, \tag{5.5}$$

where the superscript zero means zero pressure, then

$$n_v = \exp\{-(\Delta G_f^0 + pV_f)/kT\}. \tag{5.6}$$

A linear increase in pressure causes an exponential decrease in vacancy concentration.

It is in the nature of the metallic bond that the metal tends to maintain a fixed volume per free electron. If a vacancy is created by removing an ion from the interior and placing it on the surface, the number of free electrons is unchanged, and the metal contracts. For this reason, the experimentally measured values of V_f for metals are small: about $\frac{1}{2}\Omega^0$ where Ω^0 is the atomic volume Strongly ionic solids can behave in the opposite way: the removal of an ion exposes the surrounding shell of ions to mutual repulsive forces. The vacancy becomes a centre of dilatation, which is why the observed values of V_f are large: up to $2\Omega_i^0$ where Ω_i^0 is the volume of the ion removed. There are no measurements for oxides or silicates; but, when the bonding is largely covalent, one might expect the close-packed oxygen lattice which characterizes many of them (among them olivine) to behave much like an array of hard spheres. Forming a vacancy then involves a volume expansion of Ω_i^0, the volume associated with an oxygen atom in the structure.

We might, then, expect that V_f should about equal Ω_i^0, the oxygen-ion volume, in a silicate like olivine, but there is a complicating factor. In a multi-component system, vacancies may be stabilized for reasons other than those of entropy. Ionic compounds, for instance, when doped with ions of a different valency, adjust by creating vacancies of one species or interstitials of the other to maintain charge neutrality; pressure will not then change the vacancy concentration. Oxides may not be stoichiometric, even when pure, and the deviation from stoichiometry is often achieved by creating vacancies on one of the sub-lattices. The concentration of these vacancies is influenced by the activity of oxygen in the surrounding atmosphere, so that it is not the net pressure but the partial pressure of oxygen which determines the rates of diffusion. For these reasons it is possible that the quantity V_f in equation (5.6) could lie between 0 and Ω_i.

The jump frequency, too, depends on pressure. In diffusing, an ion, vibrating about a position of equilibrium, jumps to a neighbouring vacant position in which its surroundings are identical. In doing so, it passes through an activated state in which its free energy is increased by the energy of motion, ΔG_m. The frequency of such jumps is then given by

$$\Gamma = \nu \exp(-\Delta G_m/kT), \tag{5.7}$$

where ν is the vibration frequency of the atom in the ground state (and is unlikely to depend on pressure).

TABLE 5. ACTIVATION VOLUMES FOR DIFFUSION AND POWER-LAW CREEP

material	structure	V^*/Ω_i^0 for diffusion	V^*/Ω_i^0 for creep
Pb	f.c.c.	0.8 ± 0.1	0.76
Al		—	1.35
Na	b.c.c.	0.4 ± 0.2	0.41
K		—	0.54
In	h.c.p.	—	0.76
Zn		0.55 ± 0.2	0.65
Cd		—	0.63
AgBr	rock salt	1.9 ± 0.5	1.9
Sn	tetragonal	0.3 ± 0.1	0.31
P		0.5 ± 0.1	0.44

Adapted from Lazarus & Nachtrieb (1963), Goldstein *et al.* (1965) and McCormick & Ruoff (1970).

In passing through the activated state, the ion distorts its surroundings, temporarily storing elastic energy; and, if bonding is local, it breaks the bonds with some of its neighbours. In a solid with non-local bonding, like a metal, one might expect that the elastic energy would account for most of the activation energy of motion, so that (by the argument used in § 4.2) it would be associated with a maximum volume expansion,

$$V_m \approx 3\Delta G_m/2\mu, \tag{5.8}$$

per unit volume. Taking the activation energy for motion to be 0.4 of the activation energy of diffusion, we find, typically, $V_m = 0.2$–$0.4\,\Omega_i$, where Ω_i is the volume of the diffusing ion. Experimentally, V_m appears to be smaller than this, suggesting that even in metals not all the energy is elastic. And in solids like silicates with localized bonding, most of the energy of motion must be associated with bond-breaking and will not produce a volume expansion.

Assembling these results we find

$$D = D^0(1 - 2p/3K^0) \exp(-pV^*/kT), \tag{5.9}$$

where $D^0 = \alpha(a^0)^2 \nu \exp(-\{\Delta G_f + \Delta G_m\}/kT)$ and is the diffusion coefficient under zero pressure, and

$V^* = V_f + V_m$ for intrinsic diffusion;

$V^* = V_m$ for extrinsic diffusion.

Because experiments are difficult, there are few measurements of V^*, and these show much scatter. They have been reviewed by Lazarus & Nachtrieb (1963), Keyes (1963), Girifalco (1964) and Goldstein, Hanneman & Ogilvie (1965). The results are summarized in the third column of table 5, in which Ω_i is the volume of the diffusing species: they lie between 0 and $2\Omega_i$.

In summary, both physical reasoning and experiments lead to the conclusion that activation volumes could vary between zero (for a covalent solid in which diffusion is extrinsic) to perhaps

$2\Omega_i$ (for a strongly ionic solid). For silicates, in which oxygen is the slow-diffusing species, we might expect it to lie between zero (if the oxygen sub-lattice has chemically stabilized vacancies on it) and Ω_i, the ionic volume of oxygen (if it does not). These are the two limiting values used in the calculations of § 8.

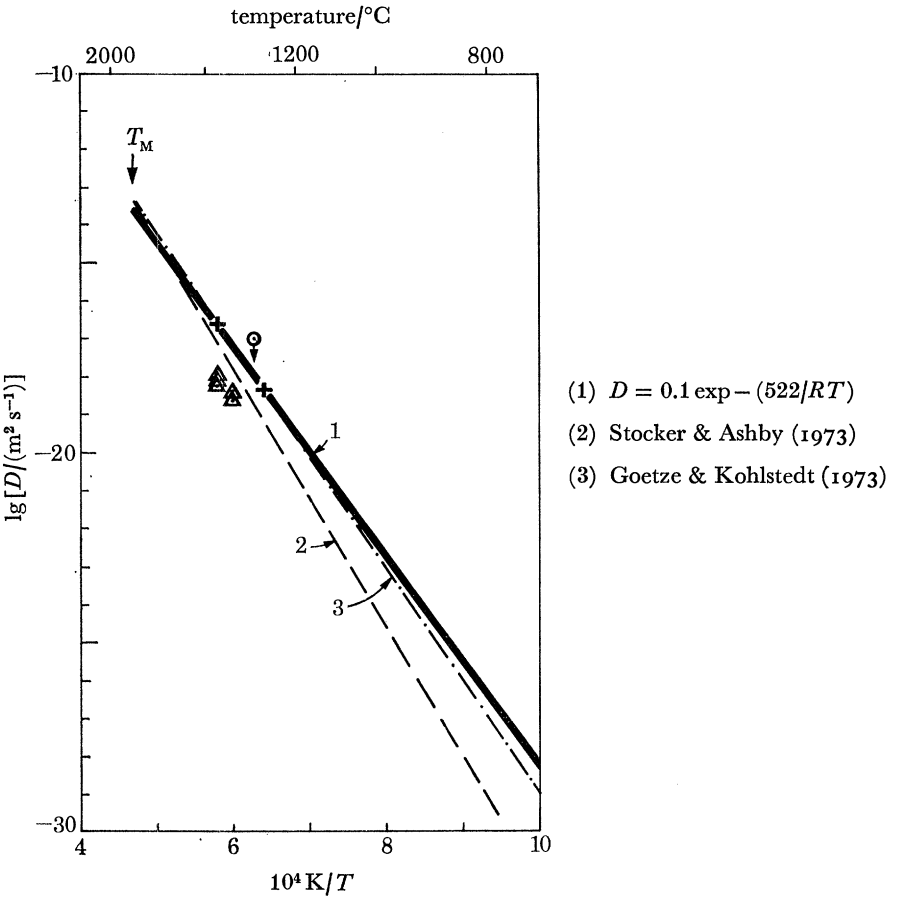

FIGURE 9. Diffusion of oxygen in olivine. The full line is a plot of the diffusion equation (equation (5.10)) used in § 8 to calculate the rates of diffusional flow. Data: +, Goetze & Kohlstedt (1973); ○, Borchardt & Schmaltzried (1972); △, Barnard (1975)

5.3. *Diffusion in olivine*

The meagre data for oxygen transport in olivine, and some attempts to fit an equation to them, are shown in figure 9. Borchardt & Schmaltzried (1972) reported that the oxygen-ion diffusivity at 1320 °C was less than 10^{-17} m²/s; Goetze & Kohlstedt (1973) inferred diffusion coefficients from the kinetics of the annealing of prismatic dislocation loops; and Barnard (1975) measured oxygen ion diffusion by a proton activation method.

Studies of power-law creep in olivine, discussed in the next section, are best described by an activation energy of $Q_{cr} = 522$ kJ/mol. If we assume that this creep is diffusion controlled, then Q_{cr} can be identified (after minor corrections for the temperature dependence of the modulus, which we shall ignore) with the activation energy for mass transport in olivine – a process which is almost certain to be limited in its rate by oxygen-ion diffusion. We have, therefore, fitted a line with this slope to the data (full line on the figure) giving

$$D/(\mathrm{m}^2/\mathrm{s}) = 0.1 \exp(-522\,\mathrm{kJ}/RT). \tag{5.10}$$

Also shown are plots of the diffusion equation proposed by Goetze & Kohlstedt (1973) (broken line), and of that by Stocker & Ashby (1973). At high temperature they are all very close, and even at low temperatures the differences are small when compared with scatter in creep and other data.

This diffusion equation predicts a melting point diffusivity for O^{2-} of $2 \times 10^{-14}\,m^2/s$, compared to an average of around $10^{-14}\,m^2/s$ for a number of other oxides which, like olivine, have a close-packed oxygen sublattice, and in which oxygen is thought to diffuse as a single ion, not a complex of ions (Stocker & Ashby 1973). Because the two numbers are similar we believe oxygen diffuses as a single ion, not as an SiO_4^{4-} complex.

There are no measurements of the pressure-dependence of diffusion in olivine, or in any other oxides. For reasons explained in the previous section, we have used two limiting values for the activation volume, V^*: zero and Ω_i, the oxygen-ion volume in olivine.

The grain-boundary diffusion parameters had to be inferred. In those materials for which both volume and grain-boundary measurements have been made, the activation energy for grain-boundary diffusion is about two thirds of that for volume diffusion. This ratio was applied to olivine. The grain boundary width was set equal to twice the average Burgers vector. Although the pre-exponential coefficient for grain-boundary diffusion is generally less than that for volume diffusion, the two were equated, somewhat increasing the importance of grain-boundary diffusion relative to volume diffusion.

5.4. *Rate equation for diffusional flow*

In the calculations of § 8, we have used equations (5.1) and (5.2), allowing Ω and Ω_1 to vary with pressure according to equation (2.1), and D to vary with pressure according to equation (5.9). The value of V^* used in each calculation is listed on the figures.

6. Power-law creep

Between the high-temperature régime of diffusional flow and the low-temperature régime of plasticity, materials – ceramics as well as metals – creep, but in a different way. The strain-rate varies as a power of the stress, the power ranging between 3 and about 10. Microscopy shows a complicated pattern of flow: superimposed on a uniform creeping of the grains is a non-uniform deformation caused by sliding at their boundaries. Electron microscopy shows that dislocations are involved; they contribute to the deformation by gliding, but, at least at high temperatures, they then aggregate to form cells. These cells have a rather small angular misorientation, perhaps 2°, between them; and their size depends on the stress. This mode of deformation is known as power-law creep. It is illustrated by figure 10.

6.1. *Diffusion-controlled power-law creep*

The origin of the power-law behaviour can be understood if the cells are thought of as little grains. Then a kind of diffusional flow is possible using the cell, instead of the grain, boundaries as sources and sinks. Because the cells are smaller, the creep rate is faster than before; and because the cell size itself depends on stress, the creep is no longer Newtonian-viscous. Observations on metals show that the cell size, d_{cell}, is, very roughly, given by

$$d_{cell}/b' \approx \mu/\sigma_s,$$

where b is the atom size, about $\Omega^{\frac{1}{3}}$. Inserting this into equation (5.1) gives the power-law creep equation:

$$\dot{\gamma} = A(D\mu b/kT)\,(\sigma_s/\mu)^n, \tag{6.1}$$

where $A \approx 21$ and $n = 3$, though we later treat them as constants to be determined by experiment.

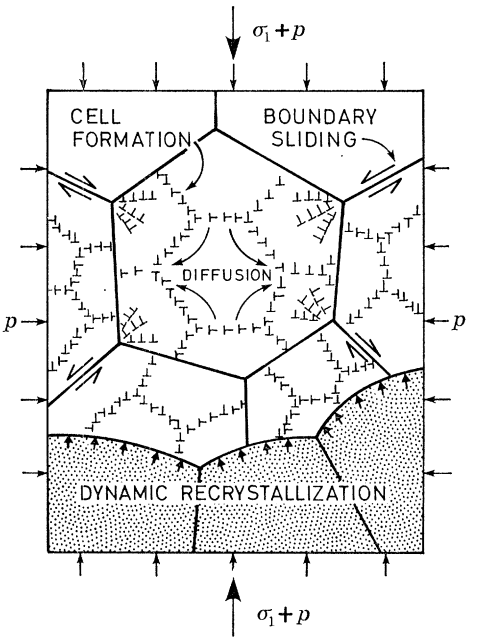

FIGURE 10. Power-law creep. The cells which form are the basis of the model described in the text, but the creep is complicated by grain-boundary sliding and by periodic recrystallization.

There are more sophisticated models for this power-law behaviour: viscous-glide creep (Weertman 1957), dislocation-climb creep (Weertman 1968), and Nabarro creep (Nabarro 1967) are examples; the characteristics of many of the models, including that given above, are discussed by Weertman (1970). All predict a steady-state creep equation of the form of equation (6.1), which varies with temperature roughly as a diffusion coefficient (usually that for lattice self-diffusion), and which depends on a power of the stress.

These models are, at best, a description of one sort of power-law creep. Their weakness lies in their inability to predict with any precision the constants A and (often) n, which must at present be regarded as empirical quantities to be determined experimentally. (The two are related; Stocker & Ashby (1973) find, in a survey of the creep of some 50 materials, that

$$n \approx 3 + 0.3 \lg A, \tag{6.2}$$

a relation which may have usefulness in estimating values of n or A when one is known, but which should be used with caution.) There are other difficulties. As the stress is raised above about $10^{-3}\,\mu$, the power-law ceases to be a good description of experiments. Physically, this 'power-law breakdown' is caused by an increasing contribution of dislocation glide to the strain-rate; it is a broad transition from pure power-law behaviour (equation (6.1)) to the exponential stress-dependence of plasticity (equation (4.1)). At high temperatures a second complication arises: the material may recrystallize as it creeps (figure 10), the waves of recrystallization washing out the cells, and giving repeated surges of primary creep.

In spite of these difficulties, equation (6.1) describes well the creep of a wide variety of metals and ceramics, provided that n and A are treated as material properties, to be determined by experiment, and it suggests that pressure should affect creep mainly through its effect on D. Experiments, reviewed in the next section, support this view.

6.2. *Effect of pressure on power-law creep*

There have been a limited number of careful creep tests in which pressure has been used as a variable; they have been reviewed recently by McCormick & Ruoff (1970). Typical of them are the observations of Chevalier, McCormick & Ruoff (1967), who studied the creep of indium under a liquid pressure medium. Their observations are replotted in figure 11. When the pressure was switched between two fixed values, the creep rate changed sharply but reversibly, returning to its earlier value when the additional pressure was removed.

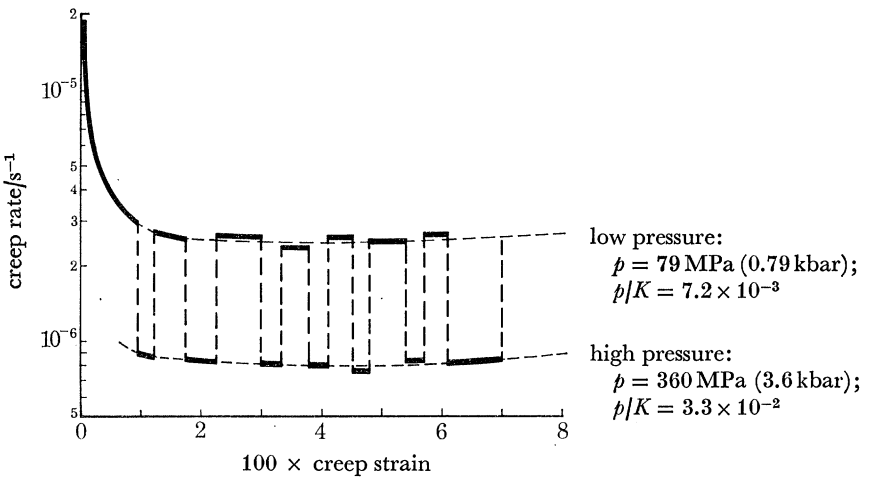

FIGURE 11. The creep of indium under a superimposed hydrostatic pressure. The creep rate drops when the pressure is applied. Data replotted from Chevalier, McCormick & Ruoff (1967): $T/T_M = 0.87$; $\sigma/E = 1.6 \times 10^{-5}$.

If the creep is diffusion-controlled, then we might expect that the main influence of pressure would be through its effect on diffusion. This is characterized by the activation volume, so that a comparison of activation volumes derived from diffusion and creep should show them to be about equal, just as the activation energies are found to be. The available data are included in table 5, where it can be seen that, when a comparison is possible, the activation volumes for power-law creep are about the same as those for diffusion.

6.3. *Creep data for olivine*

Published creep data for natural and synthetic olivines span the temperature range from 900 to 1650 °C (0.55–0.9 T_M) at strain-rates from 10^{-7} to 10^{-4}/s, often under a confining pressure of about 10 kbar (1 GPa). The results are complicated by the fact that talc was sometimes used as a pressure medium: above 800 °C it releases water, and water accelerates the creep of these (and most other) silicates. However, other experiments avoided these problems, by the use of a dry gas to apply pressure when it was required. The data in table 1 are based on these.

All investigators (Carter & Ave' Lallemant 1970; Raleigh & Kirby 1970; Goetze & Brace 1972; Post & Griggs 1973; Kirby & Raleigh 1973; Kohlstedt & Goetze 1974; Durham & Goetze

1976; Durham, Goetze & Blake 1976) observed power-law creep with a power which increased from 3 at low stresses to 5 or more at high. Many of the data were recently re-analysed by Kohlstedt & Goetze (1974), who showed them to be adequately described by the equation

$$\dot{\gamma} = f(\sigma_s) \exp(-Q_{cr}/RT), \tag{6.3}$$

where Q_{cr}, the activation energy for creep, is 522 kJ/mol.

Following their approach, we have examined the function $f(\sigma_s)$ by normalizing all the data for dry olivine to 1400 °C, using an activation energy of 522 kJ/mol, as shown in figure 12. It shows power-law behaviour, with $n \approx 3$ at low stresses, followed by a long transition as stress is raised and glide contributes increasingly to the flow.

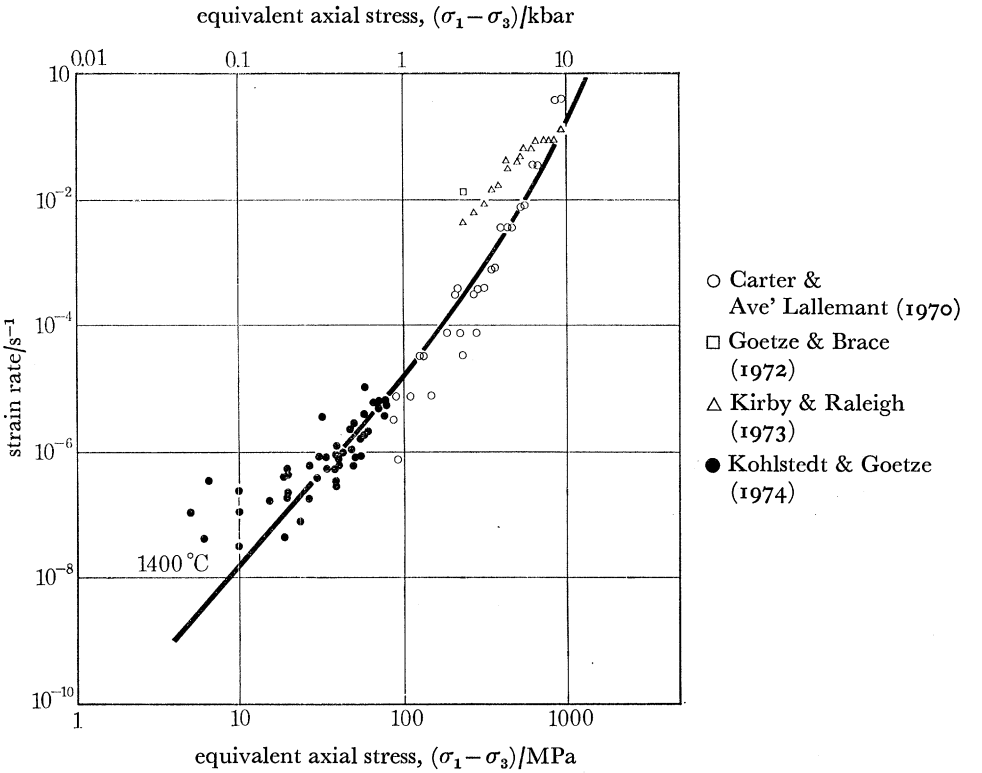

FIGURE 12. The creep of dry olivine. The data, normalized to a single temperature (1400 °C) by using an activation energy of 522 kJ/mol, are replotted from the work of Kohlstedt & Goetze (1974).

6.4. *Rate equation for power-law creep*

Because there is no convincing model for this transition, we have chosen to describe the creep of olivine by the sum of two power-laws:

$$\dot{\gamma} = \frac{\mu b}{kT}\left(A_1\left(\frac{\sigma_s}{\mu}\right)^3 + A_2\left(\frac{\sigma_s}{\mu}\right)^5\right)\exp\left(-\frac{Q_{cr}+pV^*}{kT}\right). \tag{6.4}$$

The equation, evaluated by using the constants listed in table 1, is plotted onto figure 12 as a full line, for zero pressure. In the calculations of § 8, the value of V^* was varied between 0 and Ω_i.

7. Other mechanisms

The four classes of mechanism described in §§ 3–6 are well enough understood to be modelled in broad outline, but at least three important processes are omitted from the present treatment because we do not yet understand them in sufficient detail to model them properly, and because they are too poorly characterized experimentally to be included in a phenomenological way. They are discussed in this section.

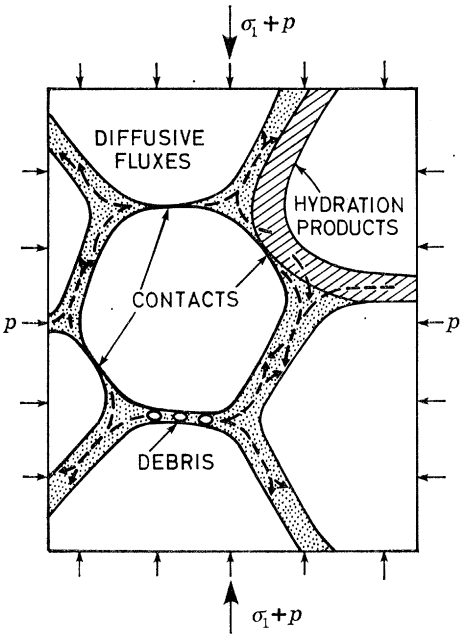

Figure 13. Fluid phase transport. A liquid film surrounding the granules: in the Earth's crust, it might be water; in the mantle, a basaltic melt. The film provides a high-mobility path for the transport of ions of the solid, permitting creep, but its thickness at the critical points of contact is hard to calculate.

7.1. *Fluid phase transport*

The pore-space of partly consolidated minerals in the Earth's crust is often filled with water. Dissolved water can change the plastic properties of individual silicate crystals, although the effect near room temperature is small. However, diffusive transport through a liquid is faster than through a solid, so that the presence of a water film between the silicate granules in the aggregate permits measurable creep by solution and re-deposition, even at ambient temperatures. Deep in the mantle, the temperature is such that water has been driven off, but basaltic phases of low melting point can provide a similar fast-diffusing liquid path (figure 13).

There have been a number of attempts to discuss and model the process (Durney 1972, 1976; Elliot 1973; Stocker & Ashby 1973; Rutter 1976). They are all based on the idea, illustrated by figure 13, that a deviatoric stress causes differences in pressure between points of contact between the granules, and that this in turn leads to a gradient in chemical potential of ions of the solid between points where the pressure is high and those where it is lower. If these ions first dissolve in the fluid and then diffuse down the gradient and re-deposit on the grains, the grains will change shape and the material as a whole will deform. The obvious parallel between this and Coble creep (§ 5) is apparent in all the models: the fluid film simply replaces the grain boundary as a high-diffusivity path.

It is in calculating the width of this path that the models are incomplete. A pressure difference can exist around the grain surface only if the liquid is at some point squeezed out, or at least reduced to a layer of little more than molecular thickness. It is only at these points that the chemical potential is significantly raised, yet it is here that the highly diffusing layer has been almost removed. The thickness of the layer and the solubility of the diffusing ions in it are crucial quantities in calculating the rate of deformation: without them, no meaningful estimate can be made.

The problem may have no easy answer. It appears to us that the most likely explanation for the observed rates of flow in the presence of water films is either that a solid hydration product forms on the grain surfaces which is porous and capable of permitting rapid ionic transport, or that porous debris – clay particles have been suggested by Weyl (1959) – lie in the interface and allow free liquid access. Both suggestions are illustrated in figure 13; they resolve the problem of liquid access to an interface under compression, but they do little to make the model quantitative.

7.2. *Dynamic recrystallization*

Above $0.6\,T_{\mathrm{M}}$, minerals, like many metals, recrystallize as they creep. The new grain boundaries sweeping through the material remove the cells and tangles of dislocations, softening the material and allowing a new cycle of primary creep (figure 10). Metals, most of which have 5 easy slip systems, creep faster when they recrystallize, though often the enhancement is slight (it depends on the number of waves of recrystallization per unit creep strain). Typical observations on metals can be found in the publications of Hardwick, Sellars & Tegart (1961), Hardwick & Tegart (1961), Stüwe (1965) and Nicolls & McCormick (1970).

Many non-metals have fewer than five easy slip systems, even at high temperatures. Although we do not understand why, there is some evidence that dynamic recrystallization may have a much more important effect on creep in these materials than it does on metals. Ice, for instance, which has two easy slip systems (those in the basal plane) appears to recrystallize locally throughout creep (see, for example, Steinemann 1958), and may in this way relieve internal stresses which would otherwise lead to cracking.

7.3. *Influence of a texture or fabric*

Mechanisms of flow involving dislocation motion may be accelerated or decelerated by the presence of a texture (which, if sufficiently perfect, tends to make the material behave like a single crystal). The creep rate depends on the degree of perfection of the texture and on the angle between the principal stresses and the preferred directions in it. We shall assume here that the texture is not sufficiently perfect to alter the creep behaviour significantly.

8. Deformation-diagrams and flow in the upper mantle

There are, then, four broad classes of mechanism of flow: cataclasis, plasticity, diffusional flow and power-law creep. All four can be studied in the laboratory, and all must be involved in the deformation of the Earth's crust and mantle, but in a given test, or at a given point in the mantle, one mechanism will be dominant, accounting for most or all of the strain. This dominant mechanism could be identified by evaluating the rate equations and comparing the strain-rate each predicts, but it is far more convenient to use the equations to construct deformation mechanism diagrams which allow the dominant mechanism to be identified, show the overall

PHILOSOPHICAL TRANSACTIONS OF THE ROYAL SOCIETY A MATHEMATICAL, PHYSICAL & ENGINEERING SCIENCES

rate of flow, and allow the depths, pressures or temperatures at which changes of mechanisms occur to be examined.

In laboratory tests the deviatoric stress, the temperature, and the pressure are all independent variables; then the kind of map described in § 8.1 is most useful. It can be regarded as characterizing the material (in this instance, olivine).

The temperature and pressure in the upper mantle, on the other hand, are related, though the nature of the relation beneath a continent may differ from that, say, beneath an ocean. Then more information is conveyed by the maps of the sort described in § 8.2.

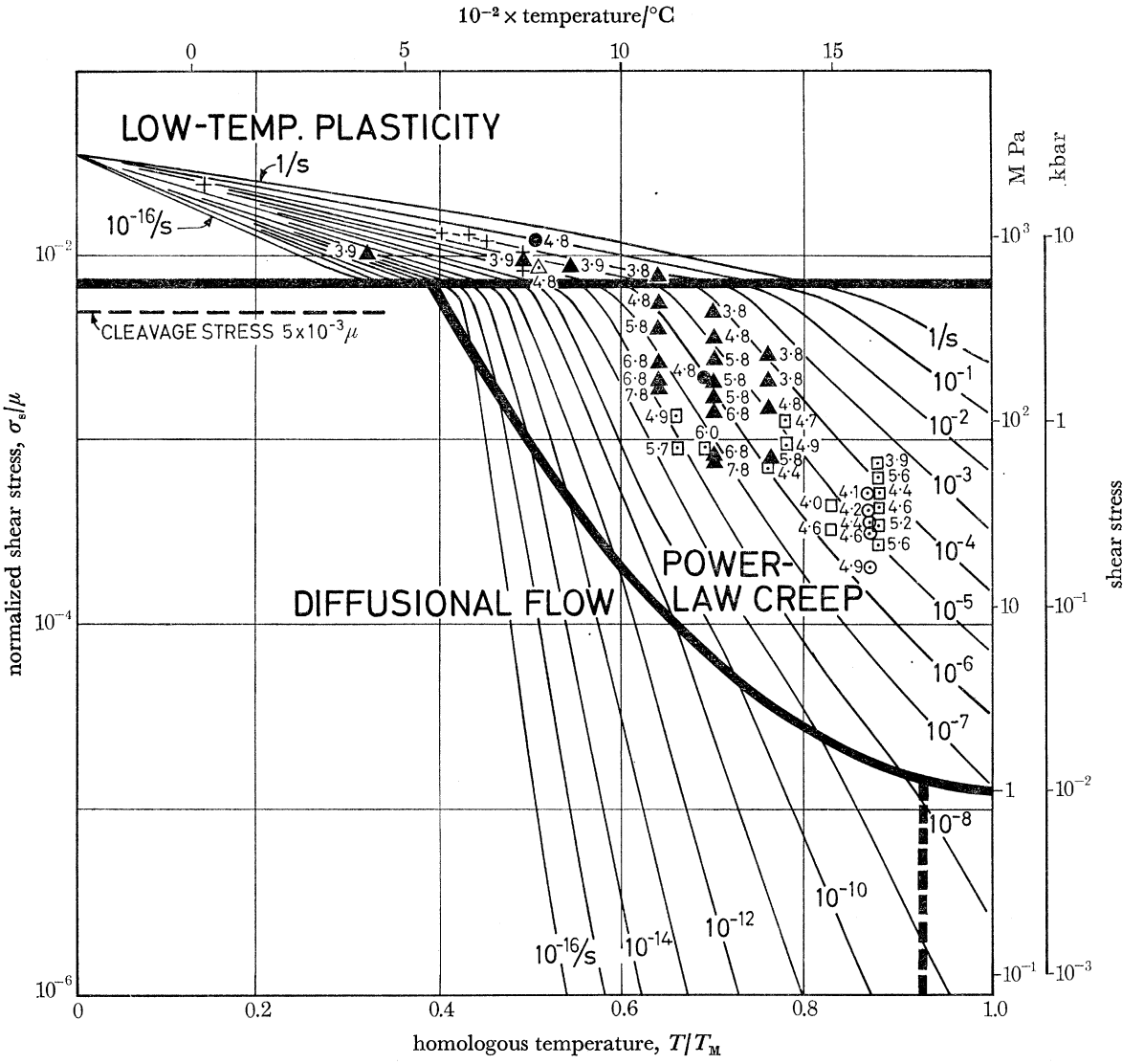

FIGURE 14. A map for olivine with a grain size of 0.1 mm; zero pressure. The symbols identify experimental points, and are labelled with the negative of the logarithm to the base 10 of the observed shear strain-rate. Cleavage was suppressed to show the plasticity field; if a realistic value for σ_i were used, the diagram would be truncated at the level marked 'cleavage stress $5\times10^{-3}\mu$'. Data: +, Evans (1976) hardness data; ▲, Carter & Ave' Lallemant (1970) (peridotite, 15 kbar); ●, Durham *et al.* (1976); △, Phakey *et al.* (1972) (single crystals, hard direction); ⊙, Kohlstedt & Goetze (1974); ⊡, Durham & Goetze (1976).

8.1. *Maps for olivine*

The first type of map is shown in figure 14. Its axes are the normalized shear stress, σ_s/μ^0 (where μ^0 is the shear modulus at atmospheric pressure and ambient temperature), and homologous temperature T/T_M (where T_M is the melting temperature). The normalization has the advantage of reducing maps for materials of the same crystal class and with similar bonding to a single group (Ashby & Frost 1975).

The construction of the maps involves two steps. We first ask: in what field of stress and temperature is a given mechanism dominant? The boundaries of the fields are obtained by equating pairs of the rate equations and solving for stress as a function of temperature. Figure 14, which describes polycrystalline olivine with a grain size of 0.1 mm, shows these fields; the mechanisms which meet at a field boundary have equal rates there. The figure was constructed from the rate equations listed in §§ 3–6 and the material constants for olivine given in table 1.

The second step is to calculate the net strain-rate at a given point on the diagram: it is the sum of the contributions from each mechanism, provided they operate independently. Cataclasis and diffusional flow are independent: at each point we add their contributions. However, power-law creep and low-temperature plasticity are not: they reflect alternative ways in which dislocations may move. In forming the sum, we include in it only the faster of these two. The superposition law implied by this procedure is obviously over-simplified, but the uncertainty in the rates of individual mechanisms makes more sophisticated superposition pointless. This procedure allows us to plot contours of constant shear strain-rate onto the diagram, from 10^{-16}/s to 1/s.

The stress axis describes either the simple shear stress or, when the stress field is more complicated, the deviatoric stress (equation (1.3)). When this and the temperature are known, the diagram gives the value of the shear strain-rate, or the equivalent shear strain-rate (equation (1.6)), and identifies the mechanism by which the material is deforming.

Figure 14 was constructed for flow under zero pressure, but with cleavage artificially suppressed (by making σ_f very large) to allow low-temperature plasticity to be shown. The map then shows three fields: plasticity, power-law creep and diffusional flow, this last subdivided by a broken line into Coble creep at lower temperatures and Nabarro–Herring creep at higher. If, instead, σ_f is set equal to $5 \times 10^{-3} \mu^0$ (the value arrived at in § 3), the diagram is truncated at the level of the horizontal line labelled 'cleavage stress'. Above this line, the material fractures when sheared under zero confining pressure.

Many of the useful data on the creep and plasticity of olivine are plotted on the diagram. The symbols identify the investigators, and are labelled with numbers which are the negative of the logarithm of the shear strain-rate (lg $\dot{\gamma}$); these numbers allow the observed strain-rates to be compared directly with those computed from the rate equations. Because there is considerable scatter in the data, we found it best to construct the maps by an iterative procedure, adjusting the constants to give a map which, in our judgement, best fitted the data. Figure 14, and the constants of table 1, are the result.

The effect of a large pressure is shown in figure 15. It was constructed for a pressure of $0.1\,K^0$ (81 kbar), roughly the pressure at the base of the upper mantle. Cleavage was not artificially suppressed, but, because of the effect described in § 3, it appears only at stress levels which are inaccessible because plasticity intervenes. The rate of plasticity has itself been slowed by a factor of 10^6 or more because of the pressure effects described in § 4, but this is equivalent to an

increase in flow stress of only a factor of about 1.5. Diffusional flow and power-law creep too, are affected, mainly because pressure slows diffusion on which both depend. Here the important parameter is the activation volume V^*, which for this figure was set equal to the volume occupied by a single oxygen ion, Ω_1. As explained in § 5, the likely range for V^*/Ω_1 is from zero (represented by figure 14) to 1 (figure 15). A comparison of the two figures shows a reduction of about 10^3 in the rate of creep.

The grain size most affects the rate of diffusional flow (§ 5): increasing the grain size slows diffusional flow and moves the boundary separating it from power-law creep to lower stresses. The grain size in the upper mantle has been discussed elsewhere (Stocker & Ashby 1973); it is unlikely to be less than 0.1 mm, and because of this the size of the power-law creep field is unlikely to be smaller than that shown on these and later figures.

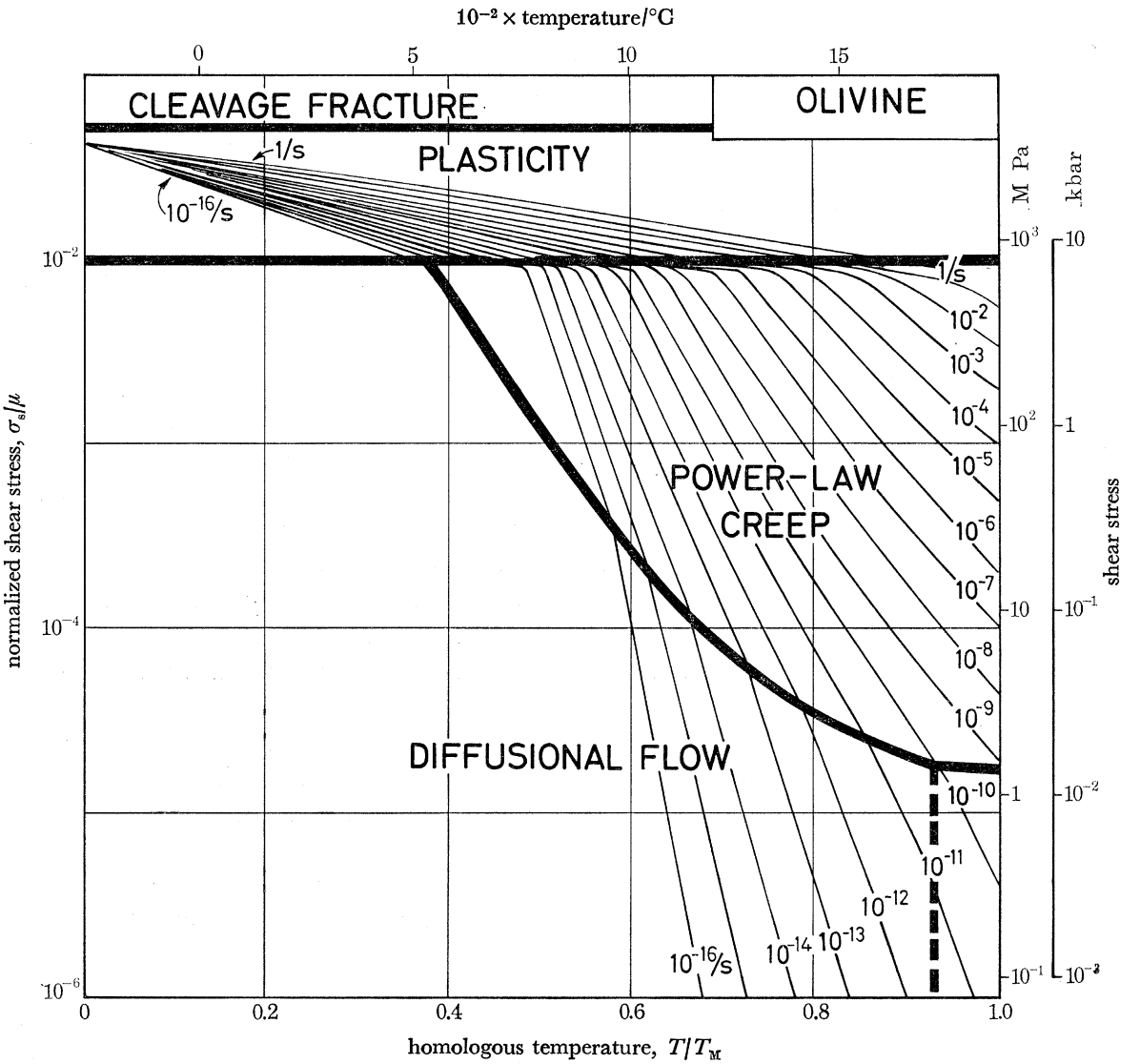

FIGURE 15. A map for olivine, based on the same data as figure 14, but with a pressure of 0.1 K^0 (81 kbar) applied. The cleavage stress has been raised by a factor of about 10 to $5 \times 10^{-3}\mu$; the stress required for plasticity has increased by a factor of about 1.5 and the creep rates have decreased by a factor of about 10^3.

8.2. *Maps for the upper mantle*

Within the upper mantle the pressure and the temperature increase with depth, the first in a roughly linear way, the second in a way which reflects the steady flow of heat from the interior to the surface. Since p and T are no longer independent, a single diagram can completely describe the mechanical behaviour. We have used depth as the independent variable, relating pressure and temperature to it by

$$p/K^0 = 7.9 \times 10^{-7} + 3.2 \times 10^4 \Delta/K^0 \tag{8.1}$$

and

$$T = 300 + 1579[1 - \exp(-7.6 \times 10^{-6} \Delta)], \tag{8.2}$$

where Δ is the depth in metres. The first equation identifies the pressure as that due to the atmosphere plus a height Δ of rock of average density 3.25×10^3 kg/m^3. The second ensures that the temperature is equal to 300 K at the Earth's surface, and increases with depth with an initial gradient of 12 K/km, reaching the value 1850 K at a depth of 500 km; it is shown in figure 16. Though reasonable, no claim is made that these equations accurately describe the pressure and temperature of a certain part of the mantle: they are meant simply to illustrate the method and the conclusions which can be drawn from it.

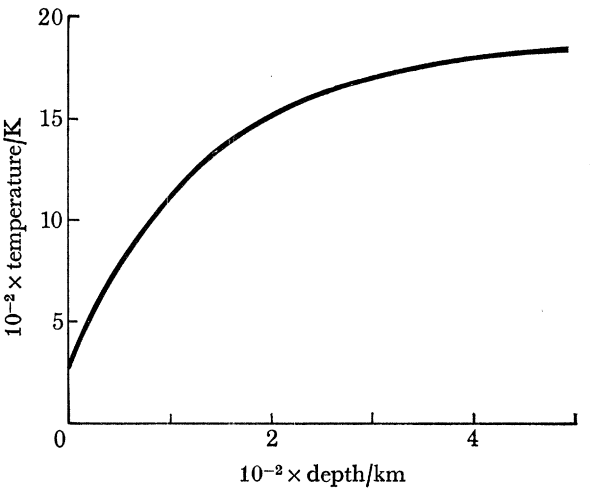

FIGURE 16. The assumed way in which temperature varies with depth in the upper mantle (see equation 8.2).

A map with depth as one axis is shown in figure 17. It describes the flow of olivine with a grain size of 0.1 mm, under conditions defined by equations (8.1) and (8.2). In constructing this figure the activation volume V^* was set equal to zero (the lower bound); it is to be compared with the next figure (figure 18) for which an activation volume equal to Ω_1 (the upper bound) was used.

The two figures illustrate the following points. Near the surface, cleavage is the dominant mode: the mantle, when sheared, will deform by cataclasis rather than plastic flow, to the depth of at least 20 km, even at the slowest strain-rates. Below this, the rising pressure and temperature combine to cause plasticity to replace cataclasis as the dominant flow mechanism. Below 100 km, power-law creep becomes important, and remains so to a depth of 400 km, where olivine transforms to a spinel-structured phase about which little is known. For this rather small grain size, diffusional flow is an important mechanism at low stresses, but if the grain size is increased to 1 mm, it disappears from the diagrams entirely.

The effects of the larger activation volume can be seen by comparing the two figures. The second, with $V^* = \Omega_i$, shows creep rates which are slower by a factor of between a hundred and a thousand than those of the first, and its strain-rate contours loop upwards slightly, because the rising pressure tends to offset the effect of rising temperature; but perhaps the most important point is that for this range of V^* the rate contours are very flat below 200 km, meaning that the viscosity of the upper mantle here is roughly independent of depth. This is in contrast to the results of earlier calculations (Stocker & Ashby 1973) which showed a pronounced viscosity minimum because they used values of V^*/Ω_i of between 3 and 7, appropriate if SiO_4^{4-} were the diffusing unit, but not if O^{2-} is the rate-controlling species (as we now believe).

The depth at which cataclasis stops and plasticity starts is illustrated by the expanded segment of figure 18 which is shown as figure 19. It illustrates first that the depth at which fracturing is

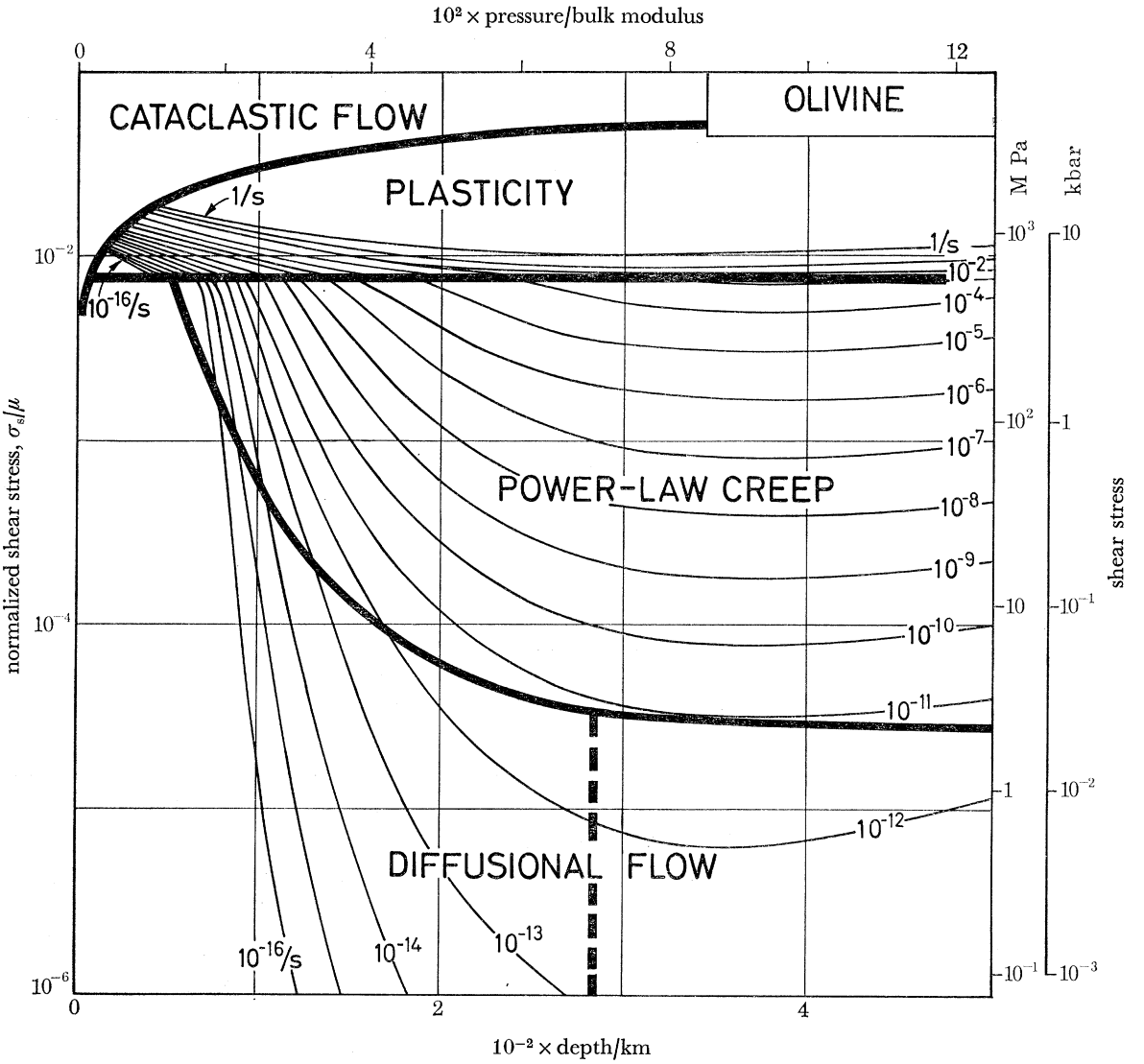

FIGURE 17. Olivine under upper-mantle conditions with $V^* = 0$; cleavage stress $= 5 \times 10^{-3}\mu$. In this figure, depth (below the Earth's surface) has replaced temperature as the abscissa; temperature and pressure are both related directly to it. The figure shows that, to a depth of about 30 km, cataclastic flow is the dominant mechanism. Below this, plasticity and creep replace fracturing as the dominant mechanisms.

replaced by plasticity depends on the local strain-rate imposed on the mantle; for our standard conditions (full lines on the figure) it is between 20 and 45 km. If we consider a standard strain-rate – say 10^{-6}/s – then the standard fracture stress of $5 \times 10^{-3}\,\mu^0$ leads to a critical depth of 32 km, and is marked by an arrow on the figure. However, this depends on the pressure and temperature distribution (equations (8.1) and (8.2)) and on the fracture stress σ_f. If the fracture stress is increased to $10^{-2}\,\mu^0$ or reduced to $2 \times 10^{-3}\,\mu^0$, (both are marked on the figure), the depth varies from 20 km to almost 50 km (arrows). It is even more sensitive to the temperature profile (equation (8.2)). The one we have used may be broadly typical of much of the upper mantle, but where, for instance, a plate is subducted and the descending matter cools its surroundings, the temperature profile is depressed and the critical depth can be displaced to below 100 km.

It is tempting to associate the critical depth with the maximum depth at which catastrophic shearing can take place, and it is certainly true that some discontinuity in behaviour must be

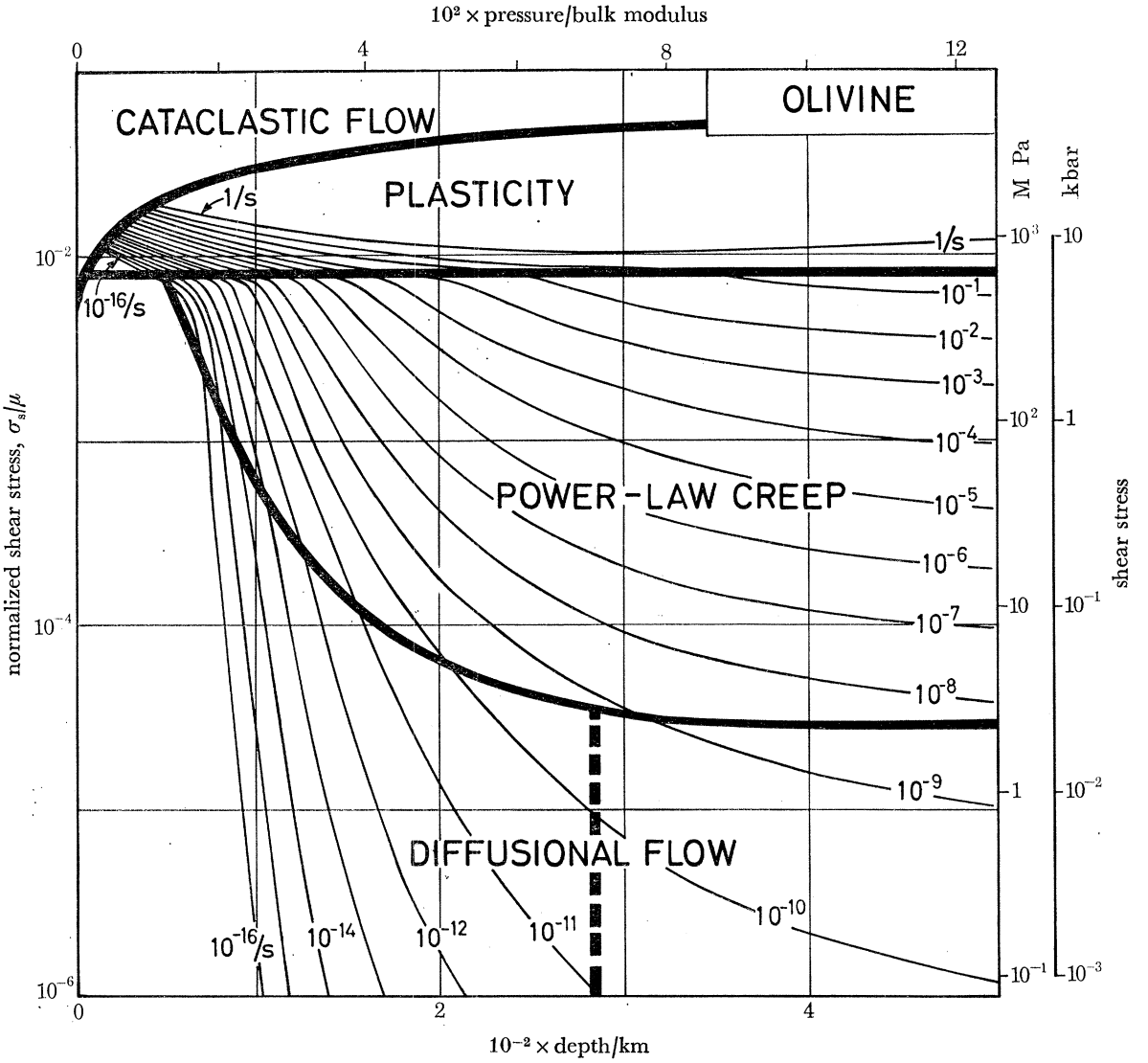

FIGURE 18. Olivine under upper-mantle conditions with $V^* = \Omega_i$. The creep rates are slower by a factor of between 10^2 and 10^3 than those of figure 17. Note that the strain-rate contours are almost flat below 200 km.

expected at this depth. However, as the olivine maps shown in figures 14 and 15 illustrate, a small increase in temperature in the plasticity régime brings with it a very large increase in strain rate: so adiabatic plastic shear, too, could lead to sudden flow.

Figure 19 also illustrates how the rolling criterion of §3 appears on the diagram. The shear stress required for rolling depends more rapidly on pressure than does that for repeated cleavage so that, while rolling is important near the surface, it does not (except for the largest values of σ_f) determine the critical depth.

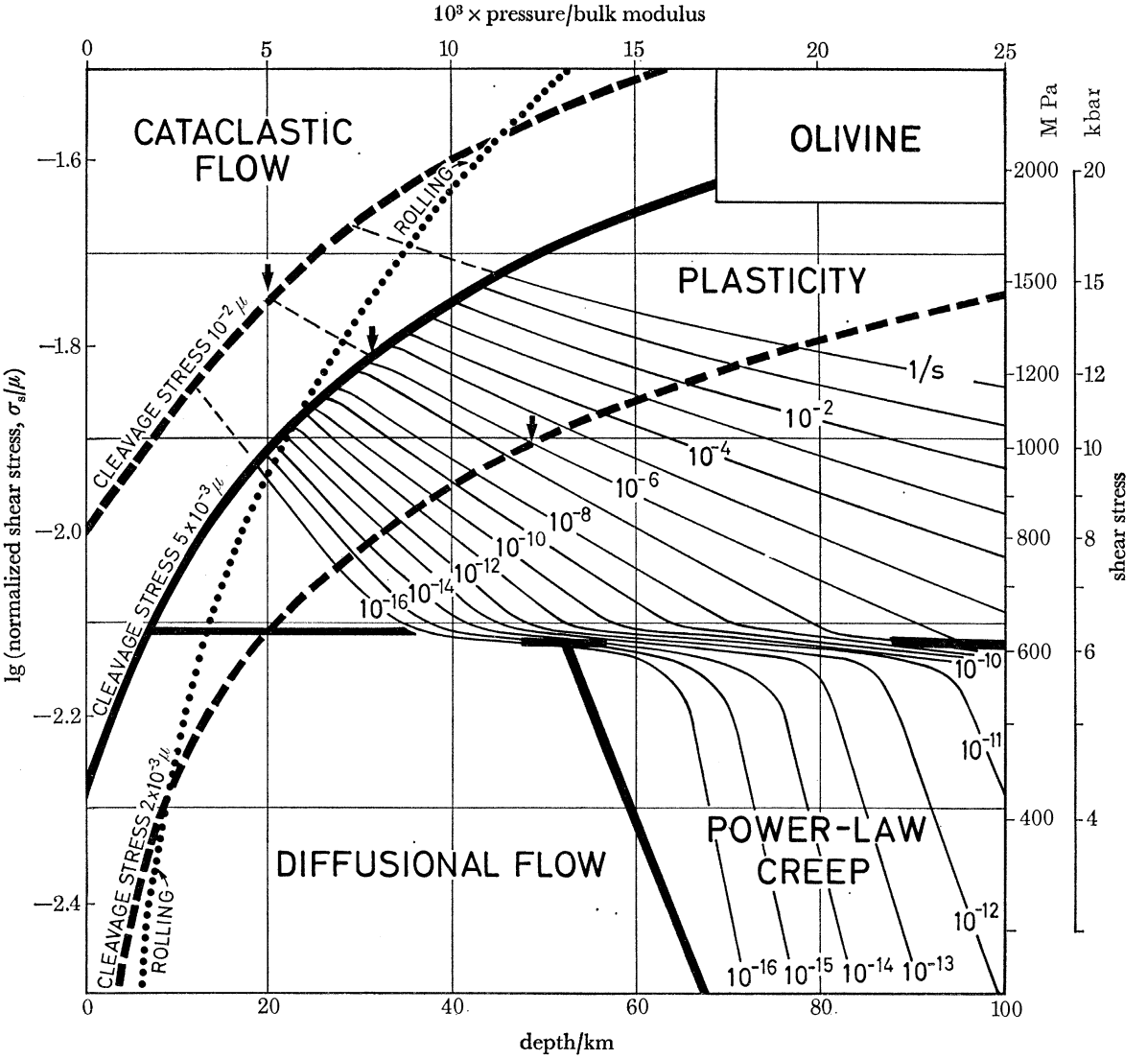

FIGURE 19. An enlarged portion of figure 18, illustrating the transition from cataclastic flow to plastic flow. The depth at which this transition occurs depends on the strain-rate and on the fracture stress, σ_f. It also depends on the temperature profile in the mantle, and will be different in regions where descending plates cool the mantle locally.

PHILOSOPHICAL TRANSACTIONS OF THE ROYAL SOCIETY A MATHEMATICAL, PHYSICAL & ENGINEERING SCIENCES

9. Summary and conclusions

A number of alternative mechanisms exist which permit flow in minerals and rocks confined by a hydrostatic pressure. Some are well enough understood that they can be modelled approximately: repeated cleavage (cataclasis), low-temperature plasticity, diffusional flow, and power-law creep are examples. Others are less well understood though they are no less important: deformation in the presence of a fluid phase, for instance; and the effects of a texture, or of dynamic recrystallization, on creep. Models for the better-understood of these mechanisms are reviewed.

The mechanical behaviour of olivine is reviewed. Recent data are analysed in the framework of the models, and methods are discussed for inferring data when none exist. A set of material properties for olivine are deduced and listed as table 1.

The models and data are used to construct deformation diagrams of two types, shows as figures 14 and 15, and as figures 17–19. The first can be regarded as characterizing the material, the second as describing its behaviour under the conditions postulated to exist in the mantle.

The study shows that olivine is now a fairly well characterized material (among oxides) and that the maps give a tolerably good description of its behaviour.

When the data and models are used to predict mantle behaviour, a number of conclusions emerge:

(*a*) Cataclasis should be the dominant mode of flow to a depth of perhaps 35 km, though this depth varies with the assumed temperature profile in the mantle, with the strain-rate, and with material properties, particularly the fracture stress σ_f.

(*b*) Below this is a region of plasticity. Because of the rapid dependence of strain-rate on temperature in this region, and the large values of stress, adiabatic instabilities are more likely here than at greater depths.

(*c*) At greater depths, the dominant flow mechanism is power-law creep, with a contribution from diffusional flow which becomes less as the activation volume is increased, and as the grain-size is increased. Diffusional flow cannot be ruled out as the dominant mechanism in mantle convection, though the most plausible values of $V^*/\Omega_i = 1$ and $d > 0.1$ mm make it seem unlikely.

(*d*) The data used here suggest that, at least below 200 km, the upper mantle viscosity is almost constant with depth, a result which may have implications for the scale of mantle convection.

This work was carried out at the University of Cambridge, and at Harvard University during 1976. One of us (M.F.A.) wishes to thank the Division of Engineering and Applied Physics at Harvard for their hospitality, help and stimulus during this period, and the other (R.A.V.) wishes to thank the Science Research Council for support on contract number B/RG 8058.8. Throughout the course of the work, we had numerous discussions with Professor R. O'Connell of the Hoffmann Laboratory at Harvard, and we wish to thank him, Professor C. Goetze, Dr B. Atkinson and Dr E. Rutter for their helpful and critical comments.

PHILOSOPHICAL TRANSACTIONS OF THE ROYAL SOCIETY A MATHEMATICAL, PHYSICAL & ENGINEERING SCIENCES

References (Ashby & Verrall)

Ashby, M. F. & Frost, H. J. 1975 *Constitutive equations in plasticity* (ed. A. Argon), p. 117. M.I.T. Press.

Ashby, M. F. & Verrall, R. A. 1973 *Acta Met.* **21**, 149.

Barnard, R. S. 1975 Ph.D. thesis, Case-Western Reserve University, Department of Materials Science and Engineering.

Birch, F. 1966 *Handbook of physical constants*. The Geological Society of America Memoir 97, section 7.

Birch, F. 1969 *The Earth's crust and upper mantle*, Geophys. Monogr. Ser. (ed. P. J. Hart), vol. 13, p. 18. Washington D.C. A.G.U.

Borchardt, G. & Schmaltzried, H. 1972 *Ber. dt. keram. Ges.* **49**, 5.

Carter, N. L. & Ave' Lallemant, H. G. 1970 *Bull. geol. Soc. Am.* **81**, 2181.

Chevalier, G. T., McCormick, P. & Ruoff, A. L. 1967 *J. appl. Phys.* **38**, 3697.

Durham, W. B. & Goetze, C. 1976 *J. geophys. Res.* (In the press.)

Durham, W. B., Goetze, C. & Blake, B. 1976 *J. geophys. Res.* (In the press.)

Durney, D. W. 1972 *Nature, Lond.* **235**, 315.

Durney, D. W. 1976 *Phil. Trans. R. Soc. Lond.* A **283**, 229.

Elliott, D. 1973 *Bull. geol. Soc. Am.* **84**, 2645.

Friedel, J. 1964 *Dislocations*, p. 25. Oxford: Pergamon Press.

Frost, H. J. & Ashby, M. F. 1973 *A second report on deformation mechanism maps*. Harvard University Report.

Girifalco, L. A. 1964 In *Metallurgy at high pressures and high temperatures* (eds K. A. Gachneider, M. T. Hepworth & N. A. D. Parlee), p. 260. Gordon and Breach.

Goetze, C. 1971 *J. geophys. Res.* **76**, 1223.

Goetze, C. & Brace, W. F. 1972 *Tectonophysics* **13**, 583.

Goetze, C. & Kohlstedt, D. L. 1973 *J. geophys. Res.* **78**, 5961.

Goldstein, J. I., Hanneman, R. E. & Ogilvie, R. E. 1965 *Trans. A.I.M.E.* **233**, 813.

Gordon, R. B. 1965 *J. geophys. Res.* **70**, 2413.

Gordon, R. B. 1967 *Geophys J.* **14**, 33.

Graham, E. K. & Barsch, G. R. 1969 *J. geophys. Res.* **64**, 5949.

Griffith, A. A. 1924 *Proc. 1st Int. Conf. Appl. Mech., Delft*, p. 55.

Griggs, D. T., Turner, F. J. & Heard, H. 1960 *Geol. Soc. Amer. Mem.* **79**, 39.

Handin, J. 1966 *Handbook of physical constants* (ed. S. P. Clark), revised edn. The Geological Society of America Memoir 97.

Hardwick, D., Sellars, C. M. & Tegart, W. J. McG. 1961 *J. Inst. Met.* **90**, 21.

Hardwick, D. & Tegart, W. J. McG. 1961 *J. Inst. Met.* **90**, 17.

Herring, C. 1950 *J. appl. Phys.* **21**, 437.

Huntington, H. B. 1958 *Solid State Physics* **7**, 213.

Jaeger, J. C. & Cook, N. G. W. 1969 *Fundamentals of rock mechanics*, p. 178. Chapman and Hall.

Kamazama, M. & Anderson, O. L. 1969 *J. geophys. Res.* **74**, 5961.

Kelly, A. 1966 *Strong solids*, ch. 1. Oxford: Clarendon Press.

Keyes, R. W. 1963 *Solids under pressure* (eds W. Paul & D. M. Warschauer), p. 71. New York: McGraw-Hill.

Kirby, S. H. & Raleigh, C. B. 1973 *J. geophys. Res.* **78**, 5961.

Kocks, U. F., Argon, A. S. & Ashby, M. F. 1976 *Prog. Mat. Sci.* **19**.

Kohlstedt, D. L. & Goetze, C. 1974 *J. geophys. Res.* **79**, 2045.

Lazarus, D. 1971 Diffusion in solids. In *Encyclopedia of science and technology*, p. 158. New York: McGraw-Hill.

Lazarus, D. & Nachtrieb, N. H. 1963 In *Solids under pressure* (eds W. Paul and D. M. Warschauer), p. 43. New York: McGraw-Hill.

Lifshitz, I. M. 1963 *Sov. Phys. JETP* **17**, 909.

Lomer, W. W. 1957 *Phil. Mag.* **2**, 1053.

Macmillan, N. H. 1972 *J. Mat. Sci.* **7**, 239.

McClintock, F. A. & Argon, A. S. 1966 *Mechanical behaviour of materials*, p. 490. Addison Wesley.

McClintock, F. A. & Walsh, J. B. 1962 *Proc. fourth U.S. Nat. Conf. on Applied Mechanics*, p. 1015.

McCormick, P. G. & Ruoff, A. L. 1970 *Mechanical behaviour of materials under pressure* (ed. H. Le D. Pugh). New York: Elsevier.

McKenzie, D. P. 1968 In *The history of the Earth's crust* (ed. R. A. Phinney), p. 28. Princeton. N.I.: Princeton University Press.

Nabarro, F. R. N. 1948 In *Strength of solids*, p. 75. London: The Physical Society.

Nabarro, F. R. N. 1967 *Phil. Mag.* **16**, 231.

Nicholls, J. H. & McCormick, P. G. 1970 *Met. Trans.* **1**, 3469.

Orowan, E. 1934 *Z. Kristallographie* **89**, 327.

Orowan, E. 1949 *Rep. Prog. Phys.* **12**, 185.

Paterson, M. S. 1974 *Proc. 3rd Int. Congress Soc. Rock Mech.*, Denver, Sept. 1974, **1**, 521.

Peterson, N. L. 1968 *Solid State Physics* **22**, 409.

PHILOSOPHICAL TRANSACTIONS OF THE ROYAL SOCIETY A MATHEMATICAL, PHYSICAL & ENGINEERING SCIENCES

Phakey, P., Dollinger, G. & Christie, J. 1972 *Am. geophys. Un., Geophys. Monograph Series* **16**, 117.
Post, R. L. & Griggs, D. T. 1973 *Science, N.Y.* **181**, 1242.
Raj, R. & Ashby, M. F. 1971 *Trans. Met. Soc. A.I.M.E.* **2**, 1113.
Raleigh, C. B. 1968 *J. geophys. Res.* **73**, 5391.
Raleigh, C. B. & Kirby, S. H. 1970 *Mineral. Soc. Am. Spec. Paper* **3**, 113.
Ringwood, A. E. 1970 *Phys. Earth Planet, Interiors* **3**, 109.
Ruoff, A. L. 1965 *J. appl. Phys.* **37**, 2903.
Rutter, E. H. 1976 *Phil. Trans. R. Soc. Lond.* A **283**, 203.
Seeger, A. 1955 *Phil. Mag.* **46**, 1194.
Shewmon, P. G. 1963 *Diffusion in solids*, p. 52. New York: McGraw-Hill.
Spitzig, W. A., Sober, R. J. & Richmond, O. 1975 *Acta Met.* **23**, 885.
Spitzig, W. A., Sober, R. J. & Richmond, O. 1976 *Trans Met. Soc. A.I.M.E.* **7A**, 1703.
Steinemann, von S. 1958 *Experimental study of the plasticity of ice.* Beiträge zur geologischen karte de Schweiz, geotechnische Series Hydrologie, no. 10.
Stocker, R. A. & Ashby, M. F. 1973 *Reviews of Geophysics and Space Physics* **11**, 391.
Stüwe, H. P. 1965 *Acta Met.* **13**, 1337.
Weertman, J. 1957 *J. appl. Phys.* **28**, 1185.
Weertman, J. 1968 *A.S.M. Trans. Quart.* **61**, 681.
Weertman, J. 1970 *Rev. Geophys. Space Phys.* **8**, 145.
Weyl, P. K. 1959 *J. geophys. Res.* **64**, 2001.
Young, C. 1969 *Am. J. Sci.* **267**, 841.

Discussion

H. H. Schloessin (*Department of Geophysics, University of Western Ontario, London, Ontario, Canada*). With regard to the deformation of bodies whose grains are in contact with a liquid phase, it would seem that Gibbs's theory of heterogeneous equilibrium of solids under all states of stress and strain in contact with their solution or melt can provide a suitable basis for its determination (J. W. Gibbs, *Collected Works*, vol. 1, ch. 3, 1928). Similar to the case of Nabarro–Herring creep the deformation will depend on diffusive transport of matter from the stressed faces to the unstressed (free) faces. However, in this particular case the transport will take place through the liquid phase and its rate will be determined by the difference in chemical activity (solubility) of the solid between stressed and free faces. The variation of steady state creep rate with stress should be proportional to the change in activity. This, I suppose, leads to a hyperbolic creep law.

E. H. Rutter (*Geology Department, Imperial College, London SW7*). During his particularly lucid review of the micromechanisms of flow and fracture, Professor Ashby referred to creep by diffusive mass transfer via an intergranular fluid phase. The microstructures which result from such diffusive transfer in low-grade metamorphic rocks are well known to geologists and are described as being due to pressure solution (see, for example, Heald 1956; Ramsay 1967). Though he mentioned the importance of diffusion path width in determining the kinetics of this process, I felt that special attention should have been given to the question of the diffusivity in the supposed intergranular fluid film. While the effective path width can probably be inferred to within one order of magnitude from microstructural observations, the greatest uncertainty in estimating the rate of rock deformation by this process must be due to uncertainty regarding the magnitude of the diffusivity (Rutter 1976). There are no relevant experimental data to assist here, and it would be wrong to use diffusivities measured for salts dissolved in large volumes of fluid. If we are reduced to guessing, errors of several orders of magnitude will arise.

Returning to the subject of the diffusion path width, it is relevant to point out that pressure solution in rocks is often characterized by the development of transgranular planar zones (stylolites), extending over many grain diameters and spaced by one or more grain diameters.

Within these zones the less 'mobile' phases, usually the phyllosilicates, become progressively concentrated. The fact that stylolite zones once nucleated are stable, suggests that very fine grained phyllosilicates provide a region of enhanced diffusivity, in part by increasing the effective path width and in part by their ability to adsorb pore water onto their surfaces (see, for example, Heald 1956).

References

Heald, M. T. 1956 Cementation of Simpson and St Peter sandstones in parts of Oklahoma, Arkansas and Missouri. *J. Geol.* **64**, 16–30.
Ramsay, J. G. 1967 *Folding and fracturing of rocks*. New York: McGraw-Hill.
Rutter, E. H. 1976 The kinetics of rock deformation by pressure solution. *Phil. Trans. R. Soc. Lond.* A **283**, 203–219.

K. H. G. Ashbee (*H. H. Wills Physics Department, University of Bristol, Bristol* 8). Transmission electron microscopy studies of deformed quartz, quartzites and other crystalline silicates demonstrate that creep at moderate temperatures (600–1000 K) and pressures (1–100 atm) is a consequence of dislocation glide mechanisms. If olivine is representative of silicates in general, your deformation map suggests that, in 0.1 mm grain size material, creep under the above conditions should be by diffusion mechanisms. Would increase of grain size (to single crystal material in the limit) extend the plasticity field to the régime for which laboratory data exist?

S. H. White (*Department of Geology, Royal School of Mines, Imperial College, London SW*7 2*BP*). Professor Ashby has made a significant contribution to olivine deformation studies by considering cataclastic flow. It is noted that this field is positioned mainly in a crustal environment. Leaving aside the question of olivine stability during other than retrograde crustal deformations, the extent of the cataclastic field could perhaps be more accurately determined if the effects of pore fluid pressure were considered. The pore fluid pressure in the crust is normally considered to equal the geostatic pressure (Turner 1968; Price 1975) and it has a pronounced effect on crustal deformation and fracturing processes (Price 1975).

Carbon dioxide may exist in large quantities in the mantle (Roeder 1965; Green 1972) and may be the important fluid phase during the deep crustal and upper mantle deformation of olivine. Bubbles containing CO_2 are present around the grain boundaries of mantle derived polycrystalline olivine rocks and they will influence grain-boundary deformation processes within the mantle and fracture processes within the crust.

References

Green, H. W. 1972 A CO_2-charged asthenosphere. *Nature Phys. Sci.* **238**, 847–852.
Price, N. J. 1975 Fluids in the crust of the earth. *Sci. Prog., Oxf.* **62**, 59–87.
Roeder, E. 1965 Liquid CO_2 inclusions in olivine bearing nodules and phenocrysts from basalts. *Am. Mineral.* **50**, 1746–1782.
Turner, F. J. 1968 *Metamorphic petrology*. New York: McGraw-Hill.

S. A. F. Murrell (*Department of Geology, University College London, Gower Street, London WC*1*E* 6*BT*). Pore pressures and dilatancy during the fracturing process play very important rôles in the deformation of rocks. High fluid pressures may exist down to considerable depths in the Earth, and by the operation of the effective stress principle (Murrell 1964, 1966; Murrell & Digby 1970), may allow fracture and cataclasis to take place at low shear stresses. On the other hand dilatancy caused by the opening of micro-cracks in rock during the fracture process, even under high confining pressures (Brace, Paulding & Scholz 1966), may when pore fluids are present under

'undrained' conditions result in dilatancy hardening, the elimination of macroscopic faulting accompanied by a stress-drop, and the development of more homogeneous processes of cataclastic deformation (Ismail & Murrell 1976). Dilatancy is also likely to play a rôle in the movement of pore fluids and therefore in the dynamics of faulting processes in the crust of the Earth (Nur, Bell & Talwani 1973; Nur & Schulz 1973).

References

Brace, W. F., Paulding, B. W. & Scholz, C. H. 1966 Dilatancy in the fracture of crystalline rocks. *J. geophys. Res.* **71**, 3939–3953.

Ismail, I. A. H. & Murrell, S. A. F. 1976 Dilatancy and the strength of rocks containing pore water under undrained conditions. *Geophys. J. R. astr. Soc.* **44**, 107–134.

Murrell, S. A. F. 1964 The theory of the propagation of elliptical Griffith cracks under various conditions of plane strain or plane stress. *Br. J. appl. Phys.* **15**, 1211–1223.

Murrell, S. A. F. 1966 The effect of triaxial stress systems on the strength of rocks at atmospheric temperatures. *Geophys. J. R. astr. Soc.* **10**, 231–281.

Murrell, S. A. F. & Digby, P. J. 1970 The theory of brittle fracture initiation under triaxial stress conditions. *Geophys. J. R. astr. Soc.* **19**, 499–512.

Nur, A., Bell, M. L. & Talwani, P. 1973 Fluid flow and faulting. 1. *Proc. conf. on tectonic problems of the San Andreas fault system* (eds R. L. Kovach & A. Nur), Geol. Sci. Series, vol. 13, pp. 391–404. California: Stanford University.

Nur, A. & Schulz, P. 1973 Fluid flow and faulting, 2. *Proc. conf. on tectonic problems of the San Andreas fault system* (eds R. L. Kovach & A. Nur), Geol. Sci. Series, vol. 13, pp. 405–416. California: Stanford University.

A. Kelly, F.R.S. (*Vice-Chancellor's Office, University of Surrey, Guildford GU2 5XH*). The question was raised in discussion: what is the limit to cataclasis, i.e. how far does the breakdown of the rock mass by repeated fracturing into smaller pieces proceed? One possible answer is suggested by experience which is described principally if not entirely in the patent literature, e.g. U.K. Patents 137,3214 (1971) and 146,4243 (1973). Mixtures of hard spheres of a wide variety of stony materials, such as chalk, glass beads, aggregate (flint) or china clay, show very high packing densities and great *ease of mixing* provided that populations containing three or four discrete sizes of particle are present in rather specific volume fractions. Such mixtures attain packing fractions of above 80 % and are easily sheared. I interpret this as indicating very small dilatancy hardening of the Reynolds type (see, for example, F. C. Frank (1966), *Rev. Geophys.* **4**, 405) and if cataclasis proceeded until such an array of particles were produced, the array would shear easily, perhaps with rather little further breakdown of particle size occurring. For the relative volume fractions of such arrays showing high packing fractions and easy mixing, the patent literature must be explored. Particles of the following approximate diameter ratios 1:3:7:14 at volume fractions of 40 %, 10 %, 10 %, 40 % show the property I have referred to. J. Ritter (1971) has described the size ratios (*App. Polym. Symp.* **15**, 239, New York: Wiley) as corresponding to those of baseballs, golf balls, acorns and sand.